Corrected, February 2, 1979

NASA Contract NAS8-33065

(NASA-CR-150880) ACCURACY ANALYSIS OF POINTING CONTROL SYSTEM OF SOLAR POWER STATION Final Report, 23 Jun. - 23 Dec. 1978 (Tennessee Univ.) 73 p HC A04/MF A01 CSCL 22B G3/15 N79-14143 Unclas 42219

Final Report

ACCURACY ANALYSIS OF POINTING CONTROL SYSTEM OF SOLAR POWER STATION

Prepared by

J.C. Hung and Peyton Z. Peebles, Jr.

Electrical Engineering Department
University of Tennessee
Knoxville, TN 37916

December 23, 1978

Prepared for

George C. Marshall Space Flight Center
NASA
Marshall Space Flight Center, AL 35812

NASA Contract NAS8-33065

Final Report

ACCURACY ANALYSIS OF POINTING CONTROL SYSTEM OF SOLAR POWER STATION

Prepared by

J.C. Hung and Peyton Z. Peebles, Jr.

Electrical Engineering Department
University of Tennessee
Knoxville, TN 37916

December 23, 1978

Prepared for

George C. Marshall Space Flight Center
NASA
Marshall Space Flight Center, AL 35812

FOREWARD

This report describes work done at the University of Tennessee, Electrical Engineering Department, during the period 23 June 1978 through 23 December 1978. The work was performed by Drs. Peyton Z. Peebles, Jr. and J. C. Hung, co-principal investigators, for the National Aeronautics and Space Administration (NASA), George C. Marshall Space Flight Center, Marshall Space Flight Center, Alabama 35812, under contract NAS8-33065. The Contracting Officer's technical representative was Mr. Joe Howell.

ABSTRACT

This report describes an initial investigation of the accuracy of the pointing control system of the solar power station. The scope of the effort was quite limited and no final accuracy figures are determined. The first-phase effort has concentrated on defining the minimum basic functions that the retrodirective array must perform, identifying circuits that are capable of satisfying the basic functions, and looking at some of the error sources in the system and how they affect accuracy. The initial effort has also examined three methods for generating torques for mechanical antenna control, performed a rough analysis of the flexible body characteristics of the solar collector and defined a control system configuration for mechanical pointing control of the array.

TABLE OF CONTENTS

ACCURACY ANALYSIS OF POINTING CONTROL SYSTEM OF SOLAR POWER STATION

1.0 THE BASIC PROBLEM

The National Aeronautics and Space Administration (NASA) has under study the feasibility of a space power station capable of converting solar power to microwave power. The microwave power would be radiated to an earth-bound receiving station that would in turn convert from microwave to direct current (dc) to alternating current (ac) power for the power grid. The ac power level would be about 5000 MW.

1.1 Satellite Power System Description

Figure 1.1-1 illustrates the system presently under study. The overall system, called the Satellite Power System (SPS), contains the power generating satellite and an earth station. Solar power is converted to dc power in a large solar panel (approximately 4.8 km by 9.6 km). The dc power is then converted to microwave power at a frequency of 2.45 GHz which is radiated to the earth in a power beam formed by a phased array antenna. The antenna is approximately circular with a diameter of about 1010 m. Power is generated within the array by 135,864 klystrons each with 50 kW of average power.

The basic radiating element of the antenna is a power module having one klystron. The size of the radiating surface of a power module varies from 1.02 m x 2.33 m to 3.4 m x 5.82 m in increments such that ten distinct sizes are available. Power modules are physically connected to form a subarray 10.2 m x 11.64 m. Therefore a subarray contains anywhere from 6 to 50 klystrons, depending upon its composition of power modules. Phasing for the whole array is accomplished at the subarray level. There are 6993 subarrays in the antenna.

Nine subarrays are connected to form a mechanical module 30.62 m x 34.92 m. There are 777 mechanical modules that finally constitute the array. By control of location and type of power modules within the array, the array illumination function can be

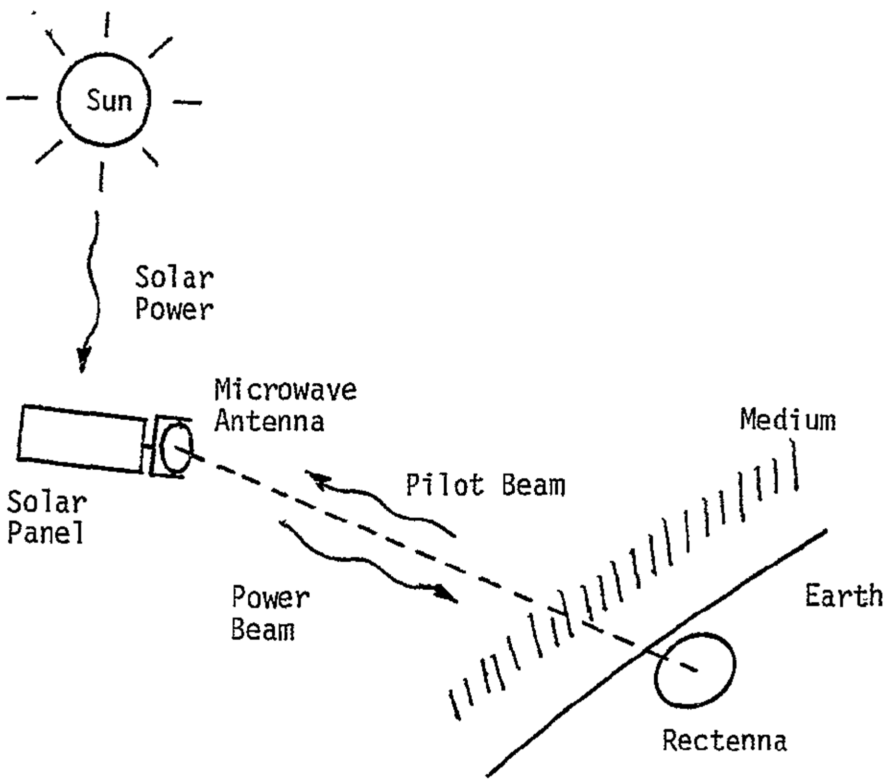

Figure 1.1-1. Illustration of the Satellite Power System (SPS).

controlled (and therefore pattern sidelobe levels).

The power beam is to be directed to a particular spot on the earth where a receiving antenna is designed to convert the microwave signal to dc by rectification. The receiving antenna is therefore called a rectenna. The dc power is finally converted to ac power at the power grid's line frequency for consumer use.

1.2 Purpose of the Study

It is necessary that the power beam have two principal properties. First, it should have as narrow beamwidth as possible with low sidelobes. Narrow beamwidth allows the rectenna to have small (relative) size and therefore low cost. Low sidelobes are required so that earth-received radiation levels outside the rectenna site are minimized both for safety and efficiency of power reception. The beamwidth/sidelobe property of the antenna is mainly determined by the illumination function derived from power module placement within the array and was not considered in this study.

The second principal property the power beam must have is stability. It must be able to point in the direction of the rectenna site and hold that direction. If the beam drifts either systematically or randomly from its desired direction, these errors, called pointing errors, can result in reduced efficiency of power transfer or the need for a larger and more expensive rectenna, or both.

It is the main purpose of this study to determine the overall accuracy to which the power beam can be directed toward the rectenna. Since the study is a first-phase effort no actual final accuracy numbers are developed. The first-phase effort has concentrated on defining the minimum basic functions that the system must perform, identifying circuits that are capable of satisfying the basic functions, and determining the errors that these circuits introduce into the overall system. In addition, several other error contributing factors are also considered.

1.3 Structure of System Studied

The study was to be conducted as free of detailed system definition as possible.

However, it is necessary to establish some minimum structure in any system for which accuracy is to be found. Because it is unlikely that a directly steered array would have the required accuracy, and because it is possible to use a cooperative source at the rectenna, it is assumed that the system uses the highly accurate retrodirective array concept.

The retrodirective array concept is described further in section 2.0. Briefly, it is a form of array that receives a signal from a pilot source located in the center of the rectenna site (the sources's antenna might be a simple paraboloidal dish of about 10 m diameter), automatically sets its phase shifters so that the power beam is transmitted in the direction from which the pilot beam signal is received. As long as the medium between the antenna and pilot source (Fig. 1.1-1) is time-stationary the retrodirective array is theoretically capable of zero pointing error. In practice, however, the medium is never perfectly stationary; there are always errors due to the presence of system noises, and various errors result from signal processing methods used within the array that degrade pointing accuracy.

It can be shown that pointing errors can result if the frequency of the pilot beam signal and that of the power beam signal are different. It will therefore be assumed that the two frequencies are the same. However, to prevent interference of the high-power array transmitted signal with the low-level received signal that is processed in the array, it will be assumed that a suitable modulation is added to the pilot beam signal at the pilot source.

It is recognized that commands, communications, and data must flow between the satellite and earth station and possibly between both of these and other satellite/earth station complexes. In this study it is assumed that these links are not part of the power beam or pilot signals.

It is well-known that large angles of beam steering in phased arrays lead to beam-broadening. In order that this effect be minimized so that its reflected size and cost increases in the rectenna be minimized, much of the physical pointing of the antenna is to be done by a mechanical gimbal which supports the array. Thus, electrical steering of the power beam is mainly used for fine-grain beam pointing.

In summary, the overall system structure includes: (1) a retrodirective phased array at the satellite with independent phasing at a subarray level, (2) a mechanical gimbal mount for the array that performs pointing of the whole array, (3) a suitably modulated pilot source at the rectenna that transmits the same nominal frequency as that of the power beam signal, and (4) no other signals are placed on the pilot or power beam signals.

2.0 RETRODIRECTIVE ARRAY CONCEPT

2.1 Description of Basic Concept

To describe briefly the action of a retrodirective array, consider a simple linear array with N receiving elements as shown in Fig. 2.1-1. Wavefronts denoted by dashed lines arrive at elements 1 and a typical element n as shown. Distances of these elements from the pilot source are R_1 and R_n, respectively. Now let the pilot source have angular frequency ω_T and transmit the signal

$$\text{wave at pilot source} = \sqrt{2P_{ps}}\cos(\omega_T t) \tag{2.1-1}$$

where P_{ps} is the average power of the source. If the time required for the typical wave to travel from the pilot source to element n is τ_n then the received signal at element n is

$$\begin{aligned}\text{signal from element n} &= \sqrt{2P_n}\cos[\omega_T(t - \tau_n)]\\ &= \sqrt{2P_n}\cos(\omega_T t - \theta_n)\end{aligned} \tag{2.1-2}$$

where P_n is the received power and

$$\theta_n = \omega_T\tau_n \tag{2.1-3}$$

is the phase delay at element n.

Next, we may write (2.1-2) in the form

$$\text{signal from element n} = \sqrt{2P_n}\cos[\omega_T t - (\theta_n - \theta_1) - \theta_1] \tag{2.1-4}$$

and observe that $-(\theta_n - \theta_1)$ is the <u>relative phase</u> of the signal at element n relative to the phase of the signal at element 1. Let element 1 be established as a <u>reference</u> signal for phase. Suppose now that circuitry at each element is able to measure $-(\theta_n - \theta_1)$ and <u>add twice the negative</u> of this phase to the received signal; a waveform with the resulting phase is then transmitted according to

$$\begin{array}{l}\text{signal transmitted}\\ \text{from element n}\end{array} = \sqrt{2P_{Tn}}\cos[\omega_T t + (\theta_n - \theta_1) - \theta_1], \tag{2.1-5}$$

where P_{Tn} is the power transmitted by element n. This waveform undergoes a phase delay $-\theta_n$ as it propagates to the rectenna. The rectenna therefore receives the signal

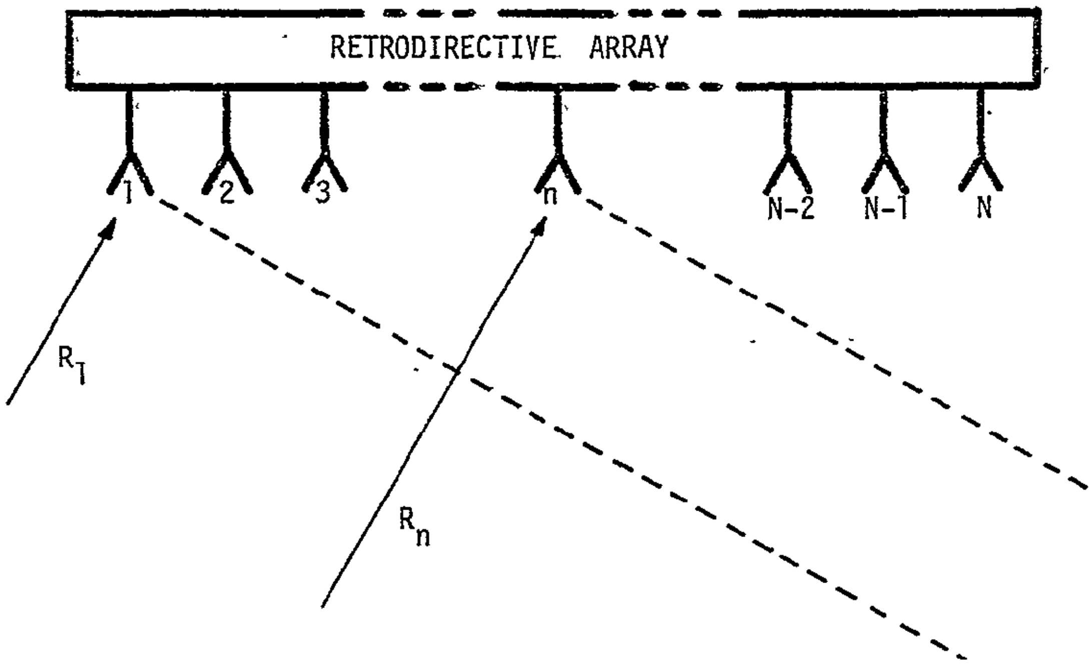

Figure 2.1-1. A retrodirective array.

$$\begin{matrix}\text{rectenna signal} \\ \text{from element } n\end{matrix} = \sqrt{2P_{Rn}}\cos(\omega_T t - 2\theta_1), \qquad (2.1\text{-}6)$$

where P_{Rn} is the received power. Since (2.1-6) is <u>independent of n</u>, <u>all</u> received radiations from the various array elements arrive at the rectenna <u>in phase</u>, which corresponds to the power beam pointing directly at the pilot source (rectenna).

2.2 Basic Functions that must be Implemented

Figure 2.2-1(a) illustrates a simple realization of the linear retrodirective array described above. It is seen that certain basic operations are performed in the system. First, the pilot signal must be separted from any interference signals that may be present (from the transmitted waveform, for example) and amplified to a useful level. This operation is called <u>pilot phase generation</u> (PPG). Second, it is necessary that the phase of the reference element be available at every other element in the array; the processing and distribution of this phase is called <u>reference phase distribution</u> (RPD). Finally, the negative of twice the relative phase $-(\theta_n - \theta_1)$ must be added to the received pilot signal's phase at each element; this process is called <u>phase conjugation</u> and is performed in a <u>phase conjugation circuit</u> (PCC). These basic functions are illustrated in Fig. 2.2-1(b).

2.3 The Required SPS Implementation

The radiators of Fig. 2.2-1 represent subarrays in SPS because that is the lowest level for which phasing (phase conjugation) is performed. The block diagram of a minimum implementation required in the SPS is shown in Fig. 2.3-1. Since a whole subarray is phase controlled all of its constituent power modules are driven from the phase conjugation circuit with the same phase. Similarly, pilot signals from all power modules must be added (in phase) to form the overall pilot signal representative of the subarray that is used for pilot phase generation.

Ideal circulators are shown in Fig. 2.3-1 to separate incoming and outgoing waves. In practice other circuits may also be used.

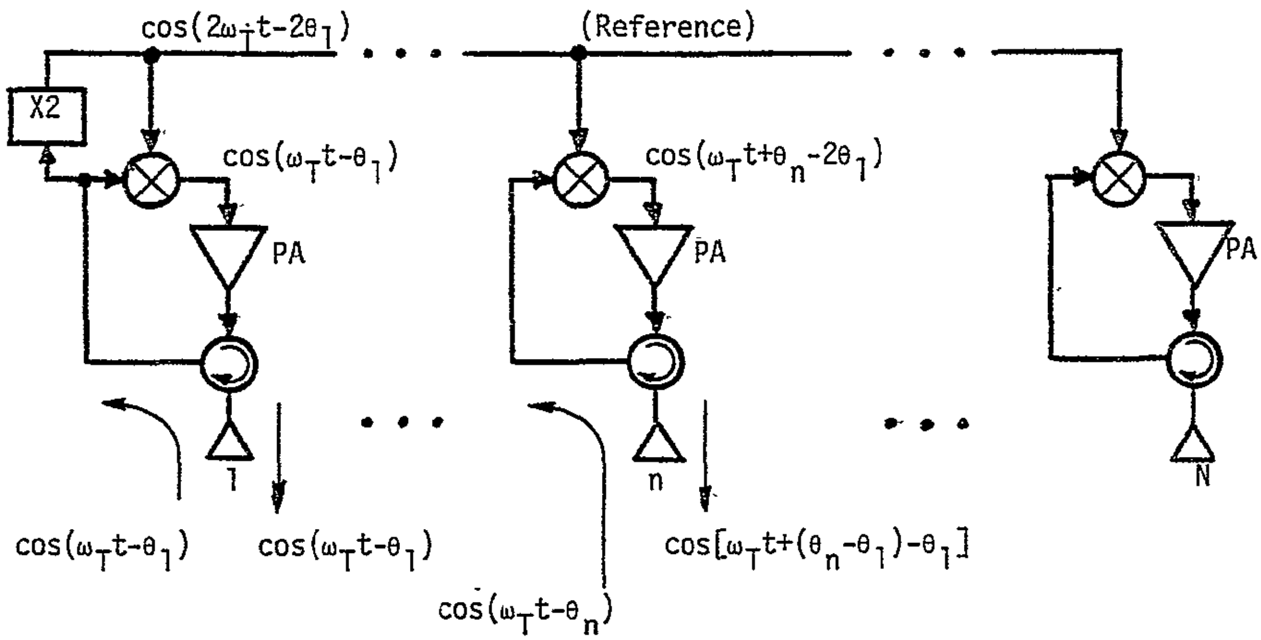

(a)

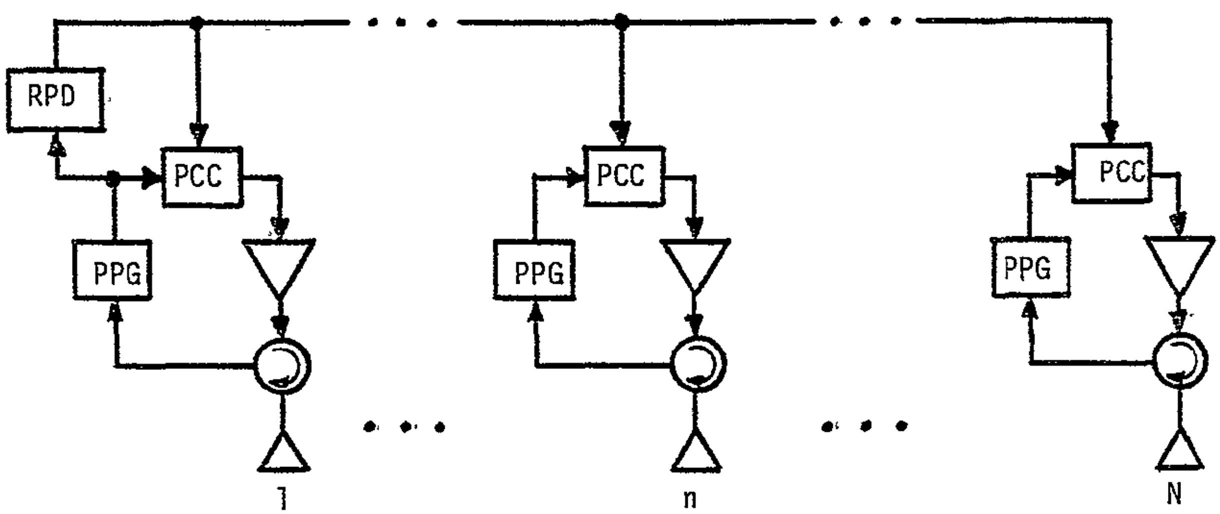

(b)

Figure 2.2-1. (a) Simple implementation of a linear retrodirective array, and (b) the basic functions that must be performed at each phase-controlled radiator.

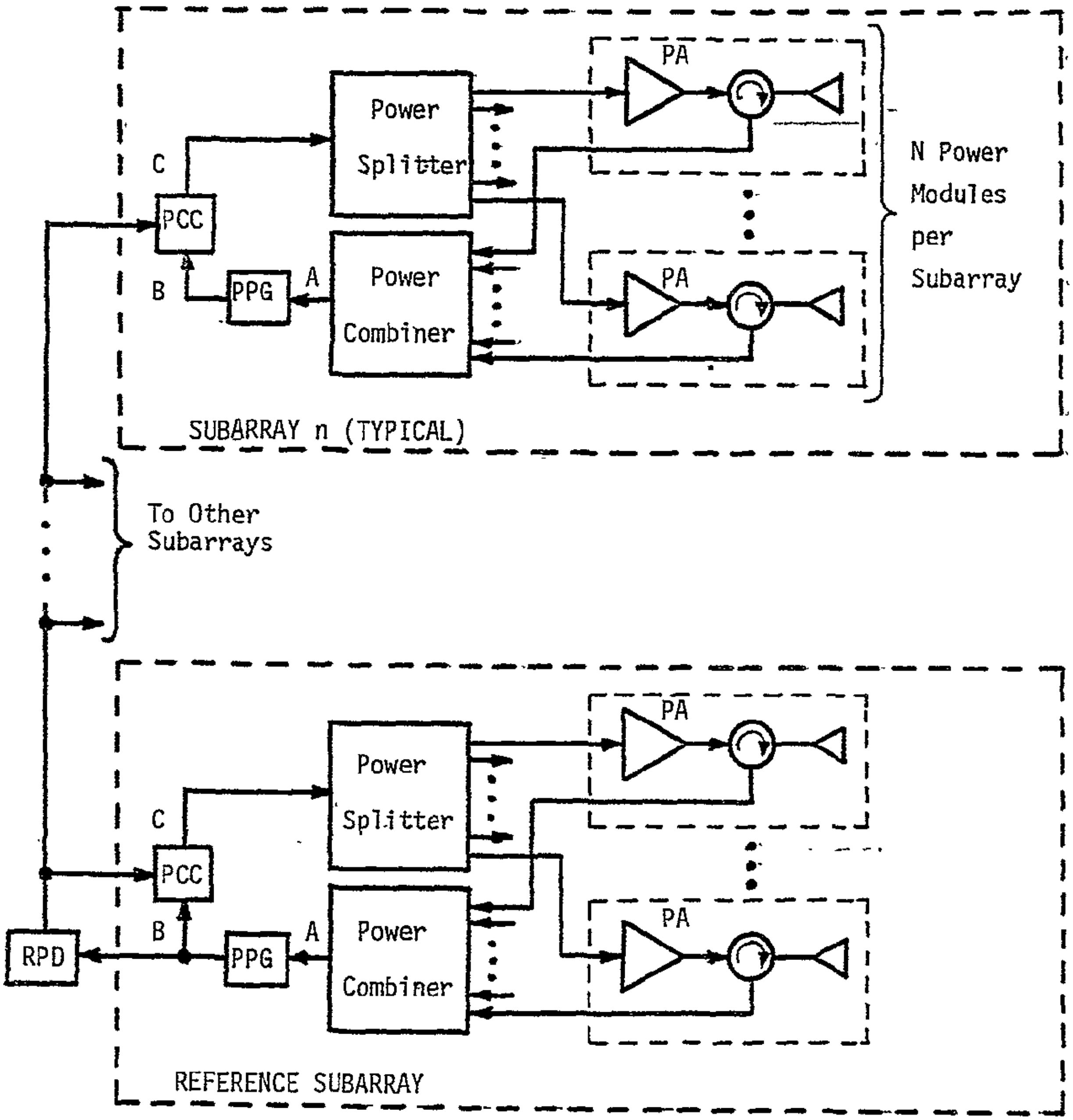

Figure 2.3-1. Implementation of a retrodirective array applicable to SPS.

3.0 RETRODIRECTIVE ARRAY COMPONENT ACCURACIES

In this section we describe some simple circuits that can be used to implement the PPG, RPD and PCC functions of Fig. 2.3-1.

3.1 Pilot Phase Generation Component

It is now shown that the circuit of Fig. 3.1-1 is capable of regeneration of the phase of the pilot signal received at the nth subarray, even in the presence of heavy leakage from the power beam.

The signal e_A is that which exists at point A in Fig. 2.3-1. It is comprised of a leakage component from the power beam at frequency $\omega_V/2\pi$, the frequency of the VCO,† plus the received pilot signal at subarray n. We shall assume the transmitted pilot signal to be of the form

$$e_p = K\{E_T\cos(\omega_T t + \theta_T) + E_p\cos(\Delta\omega t + \theta_\Delta)\cos(\omega_T t + \theta_T)\} \quad (3.1\text{-}1)$$

where K, E_T and E_p are constants. This expression is recognized as a carrier of frequency $\omega_T/2\pi$ and phase θ_T that is double-sideband suppressed-carrier modulated by a sinusoid of frequency $\Delta\omega/2\pi$ and phase θ_Δ except there is a component of carrier leakage with amplitude KE_T. Ideally, $E_T = 0$. If 1/K represents the attenuation through the medium to point A in Fig. 2.3-1, the signal e_A is

$$\begin{aligned} e_A &= E_T \cos(\omega_T t - \omega_T\tau_n + \theta_T) \\ &\quad + E_p \cos(\Delta\omega t - \Delta\omega\tau_n + \theta_\Delta)\cos(\omega_T t - \omega_T\tau_n + \theta_T) \\ &\quad + E_L \cos(\omega_v t + \theta_L) \end{aligned} \quad (3.1\text{-}2)$$

where τ_n is the delay from the pilot source to the subarray, E_L is the voltage level of the power beam leakage signal and θ_L is the phase of the leakage component. By defining

$$\Delta\theta_n = -\Delta\omega\tau_n + \theta_\Delta \quad (3.1\text{-}3)$$

---

†It will be seen as other components are discussed that the frequency of the power beam is that of the VCO if Fig. 2.3-1 is implemented from the components described in this section.

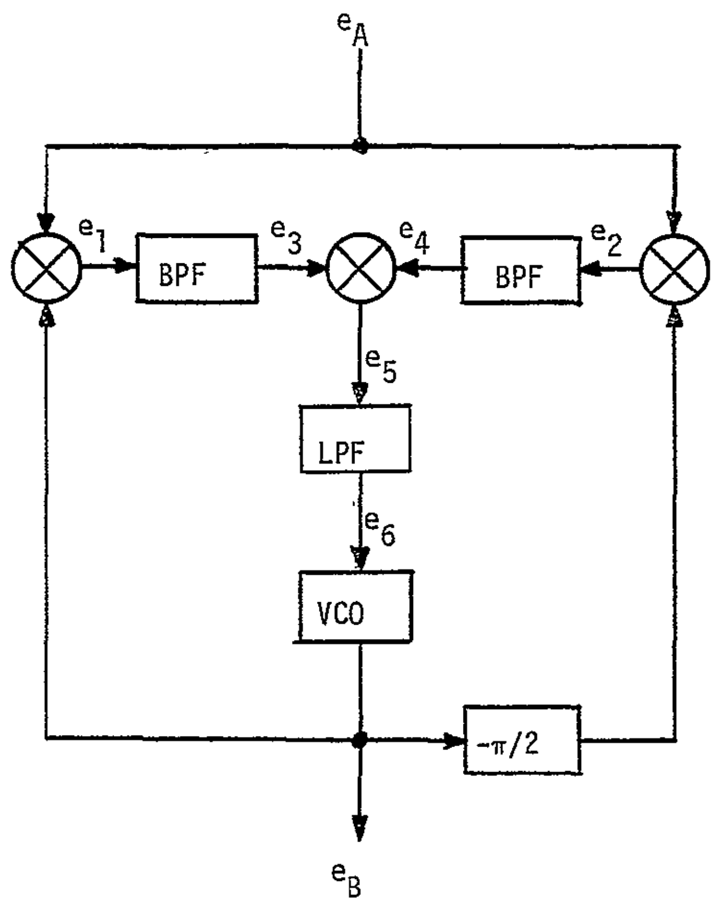

Figure 3.1-1. Block diagram of a pilot phase generation (PPG) circuit.

and using (2.3-1) we have

$$e_A = E_T \cos(\omega_T t - \theta_n + \theta_T)$$
$$+ E_p \cos(\Delta\omega t + \Delta\theta_n)\cos(\omega_T t - \theta_n + \theta_T)$$
$$+ E_L \cos(\omega_v t + \theta_L). \qquad (3.1\text{-}4)$$

The output e_B of the voltage-controlled oscillator (VCO) is

$$e_B = E_v \cos(\omega_v t + \theta_v) \qquad (3.1\text{-}5)$$

where θ_v is its phase and E_v its amplitude. After forming the products indicated in Fig. 3.1-1 and using some algebraic reduction we can write

$$e_1 = \frac{E_v E_L}{2}\{\cos(\theta_L - \theta_v) + \cos(2\omega_v t + \theta_L + \theta_v)\}$$
$$+ \frac{E_v E_p}{4}\{\cos[(\Delta\omega - \omega_T + \omega_v)t + \Delta\theta_n + \theta_n - \theta_T + \theta_v]$$
$$+ \cos[(\Delta\omega + \omega_T - \omega_v)t + \Delta\theta_n - \theta_n + \theta_T - \theta_v]$$
$$+ \cos[(\Delta\omega - \omega_T - \omega_v)t + \Delta\theta_n + \theta_n - \theta_T - \theta_v]$$
$$+ \cos[(\Delta\omega + \omega_T + \omega_v)t + \Delta\theta_n - \theta_n + \theta_T + \theta_v]\}$$
$$+ \frac{E_v E_T}{2}\{\cos[(\omega_T - \omega_v)t - \theta_n + \theta_T - \theta_v]$$
$$+ \cos[(\omega_T + \omega_v)t - \theta_n + \theta_T + \theta_v]\}, \qquad (3.1\text{-}6)$$

$$e_2 = \frac{E_v E_L}{2}\{-\sin(\theta_L - \theta_v) + \sin(2\omega_v t + \theta_L + \theta_v)\}$$
$$+ \frac{E_v E_p}{4}\{\sin[(\Delta\omega - \omega_T + \omega_v)t + \Delta\theta_n + \theta_n - \theta_T + \theta_v]$$
$$- \sin[(\Delta\omega + \omega_T - \omega_v)t + \Delta\theta_n - \theta_n + \theta_T - \theta_v]$$
$$- \sin[(\Delta\omega - \omega_T - \omega_v)t + \Delta\theta_n + \theta_n - \theta_T - \theta_v]$$
$$+ \sin[(\Delta\omega + \omega_T + \omega_v)t + \Delta\theta_n - \theta_n + \theta_T + \theta_v]\}$$
$$+ \frac{E_v E_T}{2}\{- \sin[(\omega_T - \omega_v)t - \theta_n + \theta_T - \theta_v]$$
$$+ \sin[(\omega_T - \omega_v)t - \theta_n + \theta_T + \theta_v]\}. \qquad (3.1\text{-}7)$$

If the band-pass filters (BPF) in Fig. 3.1-1 are centered at the frequency $\Delta\omega/2\pi$ and are relatively narrowband, only the first two terms in (3.1-6) and (3.1-7) that are proportional to E_p will pass through. Hence,

$$e_3' = \frac{E_vE_p}{4}\{\cos[(\Delta\omega - \omega_T + \omega_v)t + \Delta\theta_n + \theta_n - \theta_T + \theta_v] + \cos[(\Delta\omega + \omega_T - \omega_v)t + \Delta\theta_n - \theta_n + \theta_T - \theta_v]\} \quad (3.1\text{-}8)$$

$$e_4 = \frac{E_vE_p}{4}\{\sin[(\Delta\omega - \omega_T + \omega_v)t + \Delta\theta_n + \theta_n - \theta_T + \theta_v] - \sin[(\Delta\omega + \omega_T - \omega_v)t + \Delta\theta_n - \theta_n + \theta_T - \theta_v]\}. \quad (3.1\text{-}9)$$

The product e_3e_4 reduces to

$$e_5 = \frac{(E_vE_p)^2}{8}\cos^2(\Delta\omega t + \Delta\theta_n)\sin[2(\omega_v - \omega_T)t + 2(\theta_n - \theta_T + \theta_v)]. \quad (3.1\text{-}10)$$

By expansion of $\cos^2(\Delta\omega t + \theta_n)$ and consideration of the action of the low-pass filter, we have

$$e_6 \approx \frac{(E_vE_p)^2}{16}\sin[2(\omega_v - \omega_T)t + 2(\theta_n - \theta_T + \theta_v)], \quad (3.1\text{-}11)$$

where $\omega_v \approx \omega_T$.

Action of the overall loop will be to force $|e_6|$ to a small value. When stabilized the loop will have no frequency error and small phase error so

$$\omega_v = \omega_T \quad (3.1\text{-}12)$$

$$\theta_v \approx \theta_T - \theta_n \quad (3.1\text{-}13)$$

and

$$e_B \approx E_v\cos(\omega_Tt + \theta_T - \theta_n). \quad (3.1\text{-}14)$$

This last result shows that the VCO output has the phase that is received at element n when the pilot source transmits the frequency $\omega_T/2\pi$ and has a phase θ_T. In other words, the circuit of Fig. 3.1-1 has regenerated the desired pilot phase.

The actual accuracy with which phase is regenerated depends on a detailed noise analysis and loop design which was beyond the scope of the present effort.

3.2 Reference Phase Distribution Component

Once the pilot signal phase is regenerated at the reference subarray it must be distributed to other subarrays for use in the phase conjugation circuits. A suitable component is shown in Fig. 3.2-1. The reference signal with phase θ_R is to be sent to another location at distance L by some form of microwave line. At the receiving end the line is short-circuited so as to reflect most of the arriving wave back to the sending end. A small part of the arriving wave is tapped off by a directional coupler to form the useful output. A circulator separates forward and reflected waves which travel through a phase shifter with a phase shift that is a linear function of the voltage V:

$$\Delta\phi = \phi_0 + K_\phi V \qquad (3.2\text{-}1)$$

where ϕ_0 is an arbitrary constant and K_ϕ is a constant.

Assuming the reference signal's amplitude is constant V is proportional to the difference of θ_R, and the phase θ_2 of the reflected wave:

$$V = K_D(\theta_2 - \theta_R) \qquad (3.2\text{-}2)$$

where K_D is the proportionality constant. On noting that

$$\theta_2 = \theta_R - 2\Delta\phi - 2\beta L \qquad (3.2\text{-}3)$$

where β is the phase constant of the line, we may solve for the phase θ_3 of the output signal. It is

$$\theta_3 = \theta_R - \frac{\phi_0 + \beta L}{1 + 2K_\phi K_D} \qquad (3.2\text{-}4)$$

If $K_\phi K_D \gg 1$ this result shows that $\theta_3 \approx \theta_R$.

Our simple analysis shows that the distributed phase has an error $\theta_3 - \theta_R = -(\phi_0 + \beta L)/(1 + K_\phi K_D)$ which, even though small, represents a systematic error in phase arriving at a subarray. If the reference phase arriving at a given subarray has been generated by N RPD components the phase error is about N times as large as for one RPD component. The effect of these errors on pointing accuracy is difficult to deter-

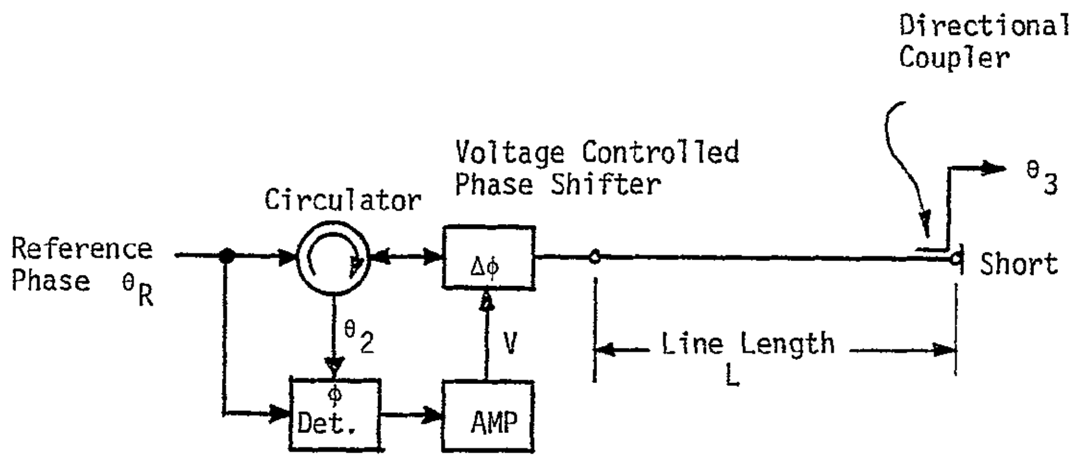

Figure 3.2-1. Reference Phase distribution circuit (RPD).

mine without knowledge of the architecture selected for reference phase distribution over the array.

3.3 Phase Conjugation Circuit Component

A possible phase conjugation circuit is illustrated in Figure 3.3-1. This circuit is compatible with the RPD component of section 3.2 and the PPG component of section 3.1. The product devices are actually mixers in practice. The reference phase θ_3 (that is the output of Fig. 3.2-1) is applied to mixer 1 along with the signal from a stable oscillator at frequency $\omega_{IF}/2\pi < \omega_T/2\pi$. The oscillator's phase is denoted θ_{IF}. The action of the mixer is to produce signals at its output that have either the sum or difference of the input phases. Thus, one has phase $\theta_3 + \theta_{IF}$ and the other's phase is $\theta_3 - \theta_{IF}$. A diplexer separates these two signals which are separately applied to mixers 2 and 3.

The signal e_B from the PPG component of Fig. 3.1-1 is also applied to mixer 2. The phase of e_B is denoted θ_B. A band-pass filter on the output of mixer 2 filters out the sum-phase component of the mixer and passes the difference-phase component having a phase $(\theta_3 + \theta_{IF}) - \theta_B$. The frequency of this component is $\omega_{IF}/2\pi$. A similar action takes place in mixer 3 except the BPF passes the sum-phase component at frequency $\omega_T/2\pi$. Its phase is $2\theta_3 - \theta_B$.

By substituting $\theta_3 \doteq \theta_R$ from (3.2-4) and θ_B obtained from (3.1-14), we have

$$\theta_{PCC} = 2\theta_3 - \theta_B \approx 2\theta_R - (\omega_T t + \theta_T - \theta_n). \tag{3.3-1}$$

However, θ_R is simply θ_B when n = 1 so (3.3-1) reduces to

$$\theta_{PCC} \approx \omega_T t + \theta_T + (\theta_n - \theta_1) - \theta_1. \tag{3.3-2}$$

If no phase errors were to exist on the RPD or PPG component outputs then (3.3-2) would be an exact equality. By comparing (3.3-2) with the phase of the nth radiator of Fig. 2.2-1(a) we see that the PCC component generates the required phase except for the constant phase angle θ_T. Because θ_T exists at <u>all</u> radiator outputs it has no affect on beam pointing accuracy.

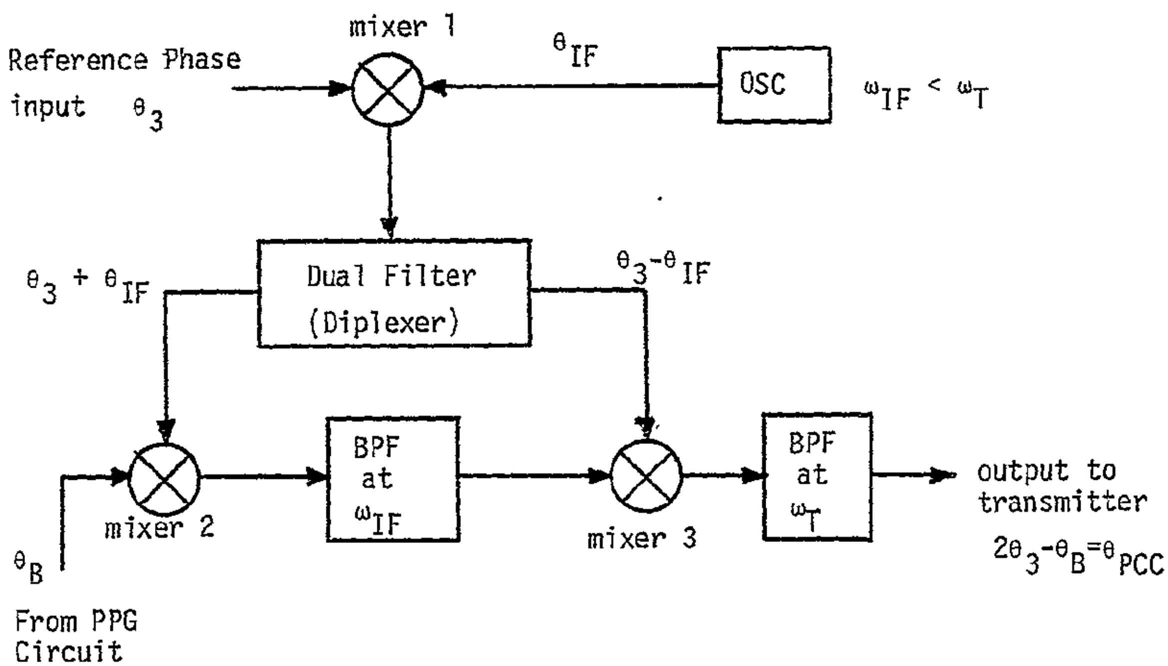

Figure 3.3-1. Phase conjugation circuit (PCC).

The PCC component can produce systematic phase errors. If the various signals between mixers undergo phase shifts $\theta_{\varepsilon ij}$, where ij represents the path from mixer i to mixer j (i = 1,2 and j = 2,3), the phase shift introduced into the output signal is $\theta_{\varepsilon 12} + \theta_{\varepsilon 13} + \theta_{\varepsilon 23}$. This phase can be nulled by an adjustable phase shifter during initial alignment so that accuracy is affected only by the phase instability of a PCC relative to others. Since each PCC is nearly identical in construction it may be possible to maintain these relative errors to tolerable values.

Phase errors introduced by the oscillator of frequency $\omega_{IF}/2\pi$ are cancelled in the output so long as the phase θ_{IF} is stable over a time equal to the time delay of the circuitry between mixers 2 and 3. This condition should be no trouble to satisfy in practice.

4.0 SOME SYSTEM ACCURACY CONSIDERATIONS

The purpose of this first-phase study has been to identify error sources and determine the manner in which they affect beam pointing accuracy. No specific final accuracy was to be developed. Rather, the effort was to be generalized, relying on additional effort to ultimately determine numerical values. Figure 4.0-1 illustrates the general flow of electrical and mechanical (dashed paths) errors in the SPS system. R and S represent random and systematic errors, respectively. We make use of this figure in discussions to follow.

4.1 Effects of Subarray Errors

The overall accuracy of a system like SPS is greatly affected by the choice of the level at which array phasing takes place. In the present system this fact equates to the choice of subarray size. Since the overall array pattern is the product of the subarray pattern and the array pattern its shape is not greatly affected by subarray size. However, as subarray size is increased grating lobes become more of a problem and the angle over which the beam can be electrically steered is decreased.

If we assume that grating lobes are no problem and the subarrays are rectangular with uniform illumination, the beamwidth corresponding to a side-length L is about

$$\text{Beamwidth} = 51\lambda/L \text{ (degrees).} \qquad (4.1\text{-}1)$$

For SPS λ = 12.24 cm, and if we use L=11.64 m, the minimum beamwidth of the subarray is 51(0.1224)/11.64 = 0.536 degrees or 32.18 $\overset{\frown}{\text{min}}$. For such a narrow beamwidth it is necessary that mechanical alignment of the planes of the various subarrays be tightly controlled over the array. To show that this may be difficult, consider Fig. 4.1-1 applicable to the array's maximum displacement in a principal mode of vibration. Displacement δh with distance ℓ from the center of the array with diameter D is

$$\delta h = \Delta h \cos(\pi\ell/D). \qquad (4.1\text{-}2)$$

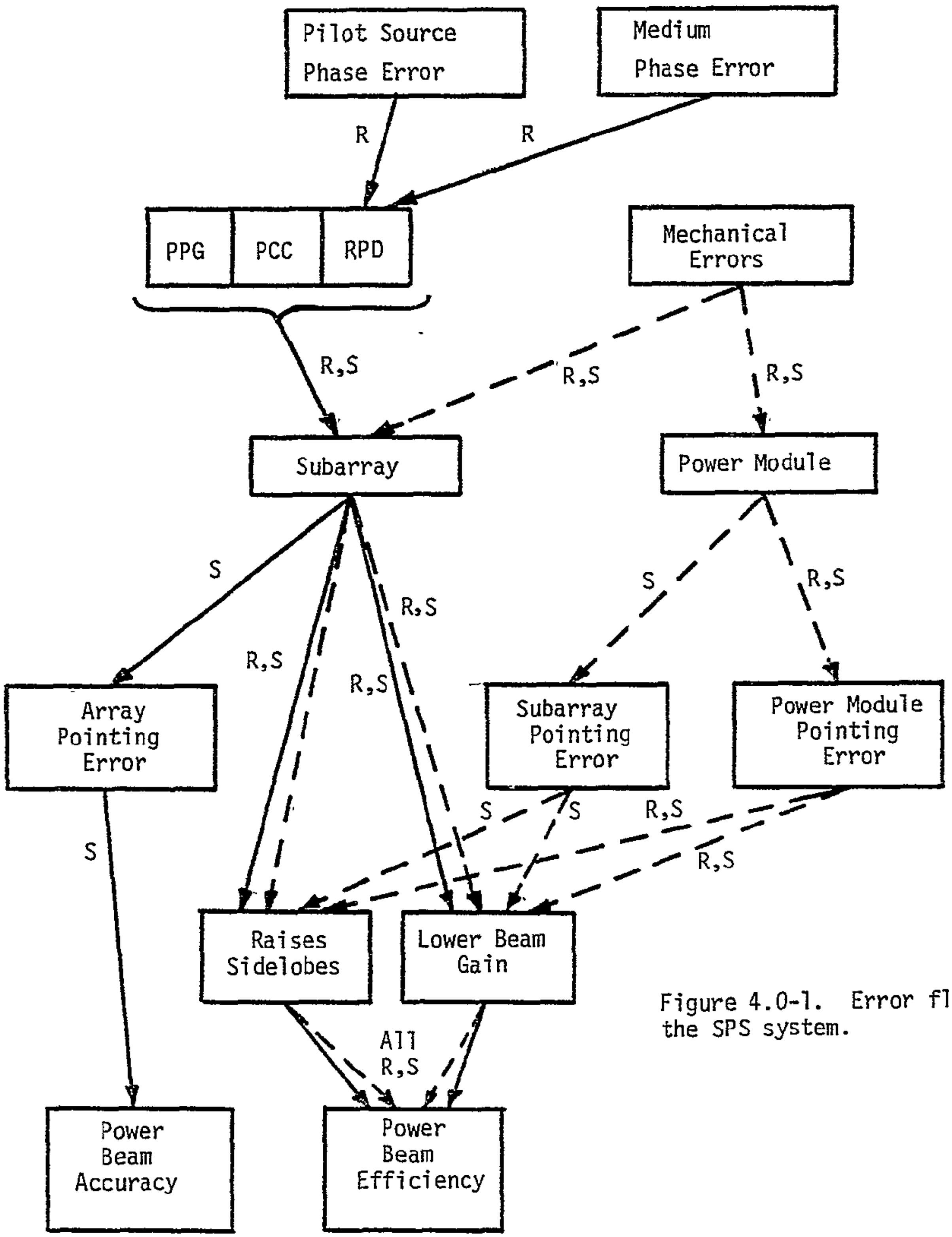

Figure 4.0-1. Error flow in the SPS system.

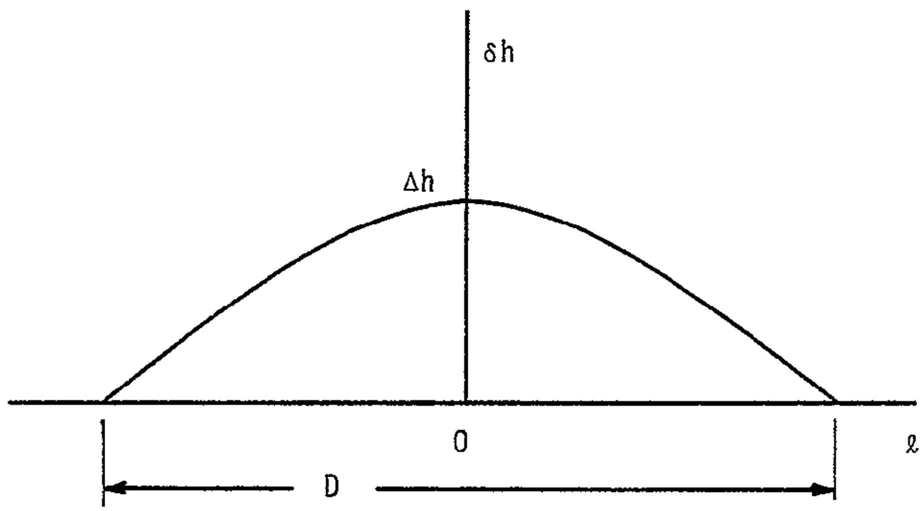

Figure 4.1-1. Vibrational displacement of array surface along a line through its center.

The slope is

$$\text{slope} = \frac{d\delta h}{d\ell} = -\frac{\Delta h\pi}{D}\sin(\pi\ell/D). \tag{4.1-3}$$

Subarrays near the outer edges of the array have their planes tilted by the maximum slope or

$$|\text{slope}|_{max} = \frac{\pi\Delta h}{D}. \tag{4.1-4}$$

If Δh = 1 m and D = 1010 m then $|\text{slope}|_{max}$ = 0.178 degrees, which is a large fraction (33.2%) of the subarray beamwidth.

Because of symmetry in the expected array vibrational modes the main effect of the resulting subarray tilt is a lowering of power beam gain and an increase in beamwidth and sidelobe radiation. Detailed calculations of these effects are difficult to make. However, it is clear that power beam broadening should be considerably less then 66.4% which is the largest that could possible occur. By using a reasonable approximation for the subarray pattern [$\sin(2.8\phi/\phi_B)/(2.8\phi/\phi_B)$ where ϕ_B is the 3dB beamwidth] the decrease in the power beam electric field intensity due to the contribution of the subarray with maximum tilt is found to be about 13.9%. However, since such subarrays are near the array's edge where their illumination is relatively low due to array taper, the overall effect in the power beam is expected to be considerably less than 13.9%.

During initial mechanical alignment of subarrays, tilt is more important than location of the subarray's face. This fact is true because action of the retrodirective array will be to automatically compensate for displacement while tilt reflects itself in noncompensateable beam broadening, sidelobe level increases, and gain reductions, as described above.

As shown in Fig. 4.0-1, the principal effect of random electrical (amplitude and phase) errors at the subarray level is to raise sidelobes and lower beam gain. These effects are difficult to calculate and have not been evaluated in this study phase. It is anticipated that evaluation will be part of the next-phase effort. Random amplitude and phase errors arise principally in the

PPG, PCC, and RPD components due to noise.

4.2 Effects of Mechanical Module Errors

As presently anticipated in SPS nine subarrays are to be connected to form a mechanical module. If the module is rigid and stable it is not clear if the concept is electrically desirable. On one hand the rigidity at a larger size "level" should tend to reduce effects of vibration. On the other hand, the rigidity may tend to "lock" tilt errors of the nine subarrays so that errors due to tilt become more systematic. In this latter case the affect on gain reduction and sidelobe increase could be worse than without mechanical modules. It would seem that adequate evaluation of the use of mechanical modules requires the development of a computer simulation.

4.3 Effects of Gimbal Errors

Errors in the mechanical pointing direction of the array face due to the gimbal cause essentially no errors in power beam pointing so long as the errors are small enough. How small is small enough depends mainly on two things: the size of the subarrays, and the amount of noise in the gimbal servos. A reasonable design would seem to require the rms noise error to be less than, say, one-tenth of the subarray's half-beamwidth. The rms noise allowance would then be about 1.61 $\overset{\frown}{\mathrm{min}}$ or 96.5 $\overset{\frown}{\mathrm{sec}}$. If additional allowances for stiction, fixed errors, etc., of about equal this value are made, the overall mechanical gimbal accuracy should be about ± 3.22 $\overset{\frown}{\mathrm{min}}$. The determination of actual errors must derive from analysis of the actual control system adopted.

4.4 Other Effects

The distribution of reference phase over the array to various subarrays requires time. The maximum of this time is that required to propagate the pilot signal phase from the reference subarray to the subarray farthest away. It can be shown that this distance is about one array radius for a reasonable phase distribution system based on a tree architecture. If allowances for circuitry and practical delay in microwave lines are made the maximum delay is probably on the order of twenty times the time required for a free-space wave to travel one array radius or 33.7 μs.

Since the phase of the transmission at any given subarray is a function of how the reference phase is distributed there are some distribution architectures that will make the array sensitive to phase stability of the medium (see Fig. 1.1-1) The extreme case would require the medium be stable in time to within a few degrees over 33.7 μs. However, it is possible to choose an architecture for which the reference phase paths to <u>every</u> subarray, even the reference subarray, are equal. This latter architecture may not be the most mass-efficient or reliable architecture but would almost entirely eliminate the time-stability problem in the medium.

Another error source due to the medium is Faraday rotation of polarization. In singly-polarized systems (such as SPS) at 2.45 GHz it is known that a polarization rotation of about 13° occurs when a wave passes through the ionosphere.† For the power beam this represents a loss in power of about 5% (-0.2 dB).

There are other effects of the medium that should be mentioned even though their analysis is beyond the scope of the present effort. They are: effects of inhomogeneities in the medium (over space and time), effects of rain depolarization and attenuation on the power beam, effects of refractivity inhomogeneities and stability, and effects of dispersion.

---

†R.S. Berkowitz (Editor), <u>Modern Radar, Analysis, Evaluation, and System Design</u>, 1965, John-Wiley & Sons, Inc., New York. See Part V, Chapter 1 by G.H. Millman (Fig. 1-23).

5.0 GIMBAL POINTING CONTROL SYSTEM CONCEPT

Because the electronic beam-steering capability of the SPS power beam is limited to only a fraction of the subarray beamwidth there must be mechanical steering of the whole array. In this section a concept is suggested as a possible means of deriving the required error signal for the mechanical gimbal servos.

5.1 The Error Sensing Concept

There is sufficient information available at the various subarrays such that only minor additional equipment is required to derive error signals for the mechanical servos. Error signals in two orthogonal coodinates are required. It is suggested that two groups of subarrays near the center of the array be used. Each group forms a small linear array in one coordinate as illustrated in Fig. 5.1-1.

Since reference phase and subarray pilot signal phase are available at each subarray from the RPD and PPG components, respectively, these may be used to derive error signals. The necessary processor is shown in Fig. 5.1-2. The signal e_n is

$$\begin{aligned} e_n = & - \cos[\theta_n - \theta_1 + (n - 1)\, \theta_q] \\ & + \cos[\theta_n - \theta_1 - (n - 1)\, \theta_q] \end{aligned} \qquad (5.1\text{-}1)$$

where θ_n is the phase delay from the pilot source to the nth element in the line of N subarrays, θ_1 is the phase delay to the first subarray (taken as the reference phase here for simplicity of discussion), and θ_q is an increment of phase shift purposely introduced between subarrays.

By summing N signals (5.1-1), it can be shown that the sum, denoted ε_2, for axis 2, is

$$\varepsilon_2 = \sum_{n=1}^{N} e_n = \frac{\sin[(N - \frac{1}{2})(\Delta\theta - \theta_q)]}{\Delta\theta - \theta_q} - \frac{\sin[(N - \frac{1}{2})(\Delta\theta + \theta_q)]}{\Delta\theta + \theta_q} \qquad (5.1\text{-}2)$$

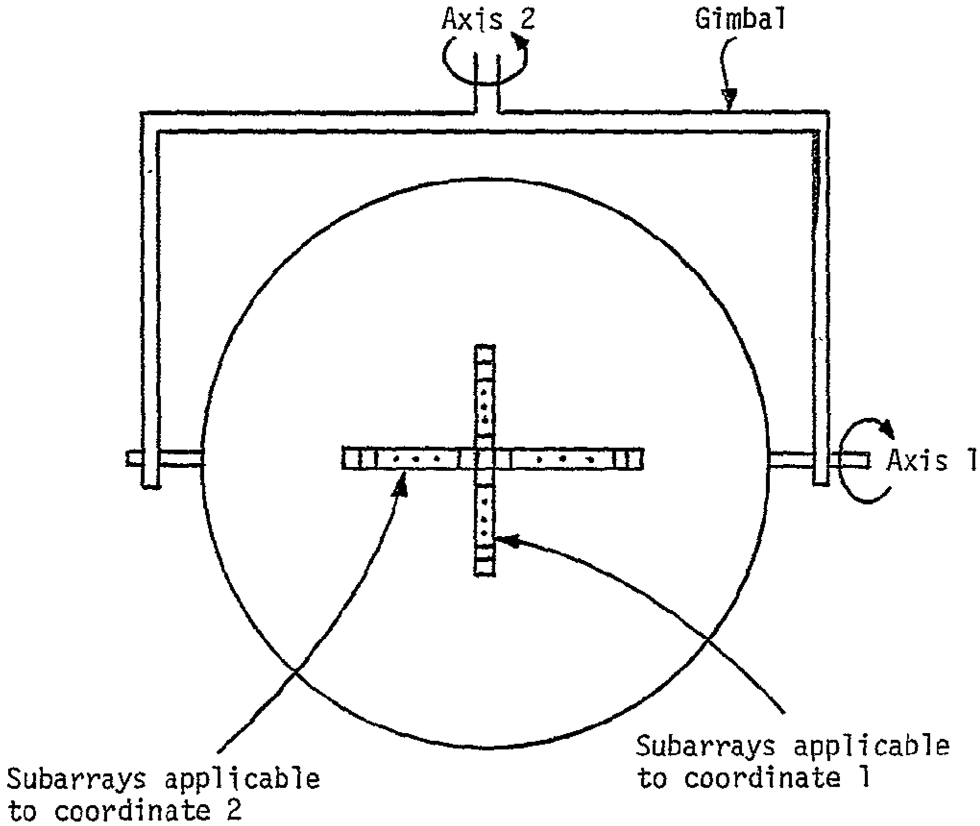

Figure 5.1-1. Subarrays applicable to gimbal servo error generation.

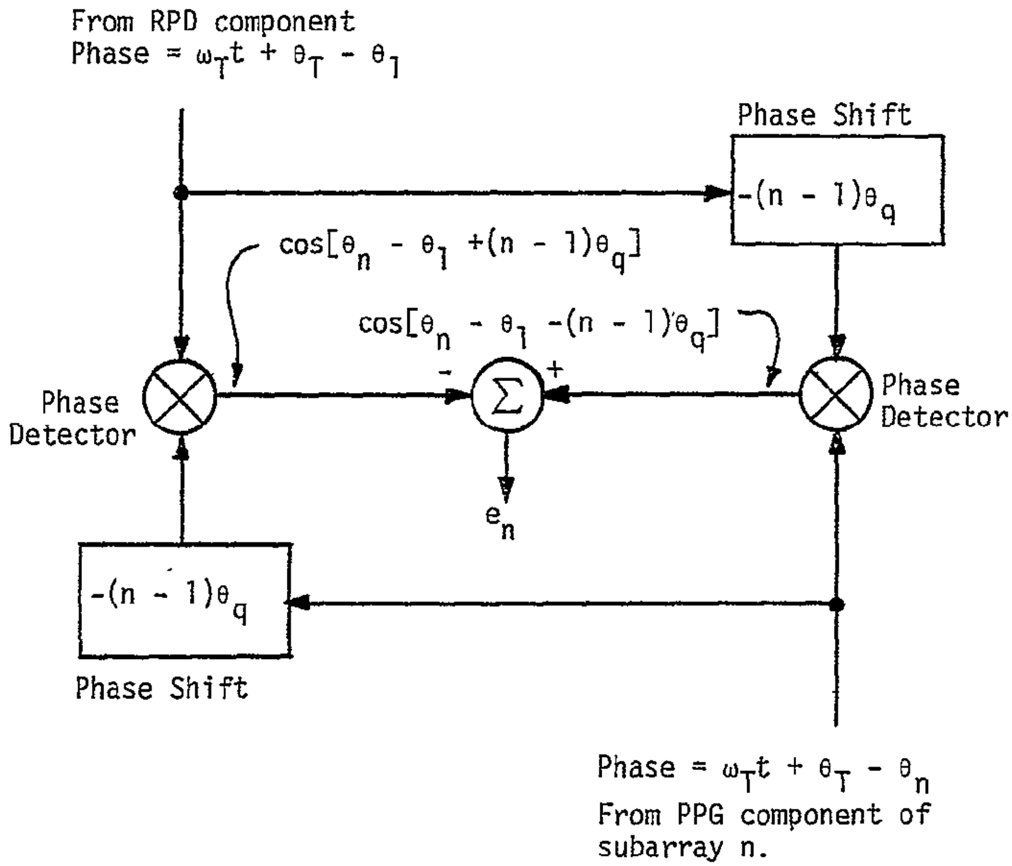

Figure 5.1-2. Signal processor at subarray n for gimbal servo error generation.

where

$$\Delta\theta = \frac{\theta_n - \theta_1}{n - 1} = \frac{2\pi D_\varepsilon}{\lambda} \sin(\phi_2), \tag{5.1-3}$$

D_ε is the separation between subarrays, λ is wavelength, and ϕ_2 is the angle of the pilot signal wavefront from the array plane in coordinate 2 (error angle).

By sketching (5.1-2) it is found that a typical servo error pattern results when ϕ_2 is small. By choice of θ_q the slope of the error pattern can be controlled. This slope is larger as N is made larger so that some N will exist that gives good gimbal servo sensitivity.

5.2 Other Discussion

Although the above treats only one coordinate, the performance in the other coordinate is similar. In the actual system, however, additional study would be needed to determine how to eliminate the reference subarrays in the two linear groups so that the reference phase of the whole array could be used instead.

From a flexure (vibration) standpoint the center of the linear group of arrays should be in the center of the array. More analysis needs to be done to determine the effects of nonflatness in each linear array group.

6.0 MECHANICAL POINTING CONTROL

6.1 Mechanical Pointing of Antenna Disc

Analysis of the pointing accuracy of the electronic phased array leads to a mechanical pointing accuracy requirement of ± 3 arcminutes for the SPS antenna disc. This 3-arcminute pointing accuracy will be achieved by mechanical control of antenna gimbal angles.

Functionally there are three types of mechanical controls for the SPS satellite, namely, "station-keeping", "attitude control", and "pointing control". The purpose of stationkeeping is to maintain a geostationary equatorial orbit and a proper spacing with respect to other satellites in the presence of outside perturbation forces. These perturbation forces include the effect of the Earth's gravitational anomalies, lunar and solar gravitational perturbations, and solar pressure. Stationkeeping is done by using a thruster type of reaction control system (RCS). The purpose of attitude control is to achieve a desired orientation of the SPS satellite so that its solar collector is pointed to a desired direction for solar energy collection, and in this method the antenna is nominally pointed to the rectenna on the ground. Disturbance sources for attitude control include the Earth's gravity gradient torque, solar pressure gradient torque, and attitude perturbations caused by stationkeeping maneuvering. Attitude control is also accomplished by RCS. The purpose of mechanical pointing control is to maintain the pointing direction and stability of the antenna disc to an accuracy required by the range of pointing operations of the electronic phased array. This control consists of two components: (1) the nominal pointing control which orients the antenna disc in a predetermined way following the rotation of earth, and (2) the reaction control to disturbances. Disturbance sources for pointing control include the anomalies in nominal pointing control, the effect of bearing friction, and perturbation caused by attitude control and stationkeeping. The mechanical pointing control is accomplished by rotating the antenna and gimbal.

Mechanical pointing control amounts to the vernier control for the antenna's pointing attitude. While an attitude perturbation of one degree is probably tolerable by solar collectors (a change of efficiency by .02%), the attitude accuracy of antenna must be maintained within ± 3 arcminutes. Therefore, pointing control relaxes the requirements of the satellite's attitude control. Our present attention is at pointing control.

6.2 Antenna-Gimbal Mechanism

Fig. 6.2-1 depicts the concept of antenna-gimbal mechanism for mechanical pointing control. Two degrees of rotational freedom are provided; namely, the rotation of the antenna disc about a fixed axis lying on the disc and the rotation of gimbal frame about its respective axis. This arrangment is capable of pointing attitude in any direction.

Three coordinate frames are defined as shown in Fig. 6.2-1;

1. Antenna frame (X_a, Y_a, Z_a)
2. Gimbal frame (X_g, Y_g, Z_g)
3. Collector frame (X_c, Y_c, Z_c)

In this figure the two rotational angles θ_a and θ_g are also defined. θ_a is the rotation of the antenna about the X_A axis and θ_g is the rotation of the gimbal about the Z_G axis. The references for angle measurements are so chosen that, when $\theta_a = 0$ and $\theta_g = 0$, all three coordinate frames have the same attitude orientation. Ideally, the Y_A axis of the antenna should be aligned in a center-to-center line between the antenna and rectenna. This alignment is achieved by controlling angles θ_a and θ_g by interpretation of certain error signals.

6.3 The Nominal Mechanical Pointing Control

The required nominal mechanical pointing control depends on the satellite orbit and the solar collector attitude chosen. The base-line orbit for this study is the "geosynchronous equatorial orbit" where the satellite stays in the

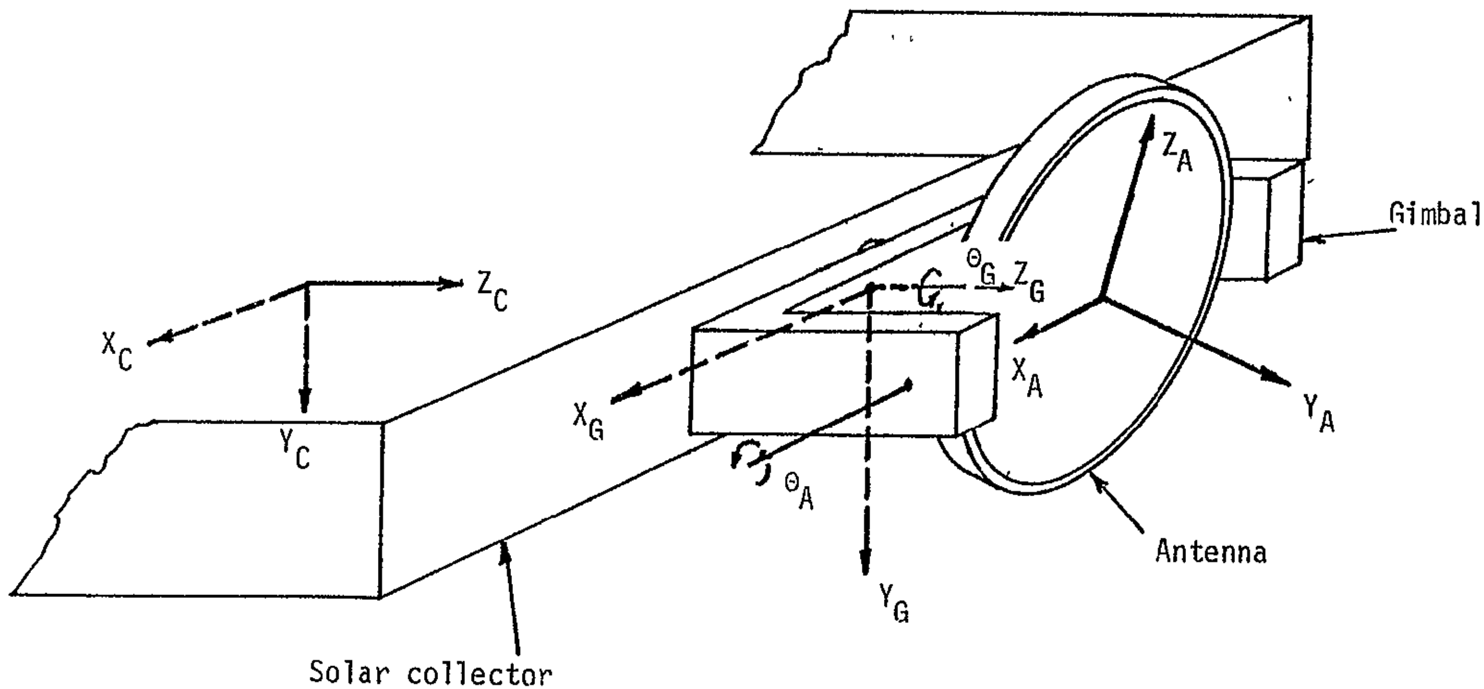

Figure 6.2-1. Antenna gimbal mechanism

equatorial plane while orbiting synchronously with the Earth's rotation. Two attitudes for the solar collector in this satellite orbit will be discussed: the "zero-gravity-gradient" attitude and the "nine-degree tilt" attitude.

Zero-Gravity-Gradient Attitude. Refer to Fig. 6.3-1(a). The longitudinal axis (Z_c-axis) of the solar collector in this arrangement is horizontal and pointing northward. The X_c-axis of the collector is maintained perpendicular to the direction of the solar rays. Under this condition, the gravity-gradient torque experienced by the collector is zero, resulting in the saving of attitude control fuel. The collector plane in this figure is making an angle of 66.6° from the direction of solar ray, which suffers from a loss of collector efficiency of 8.2% as compared to the case where the collector plane is normal to the direction of solar ray. This attitude is attractive from the nominal pointing control point of view. Under the ideal situation of zero perturbation, the antenna does not need control about its axis and the gimbal is rotating freely about the Z_g-axis at a speed of one revolution per 24 hours. If bearing friction is negligible, perpetual pointing without further control is achieved once the gimbal rotation reaches its desired steady state. Therefore, energy for nominal pointing control is not needed. Furthermore, the dynamic response of the solar collector will not affect antenna pointing when gimbal and antenna torquers are not actuated.

Nine-degree Tilt Attitude. In this arrangement, the X_c-axis of the collector is again perpendicular to the direction of the solar rays, but the collector plane is making an angle of 75.6° from the solar rays. The Y_cZ_c-plane maintains the direction of North. Fig. 6.3-1(b) shows the arrangement. The merit of this attitude is a gain of solar collector efficiency of 5.1% as compared to the previous attitude. The need of gravity-gradient torque correction fuel is offset by the saving of solar pressure correction pull. However, this arrangement requires more energy for nominal pointing control, since the steady state antenna pointing cannot be maintained by free rotation. Consequently, antenna pointing can not be

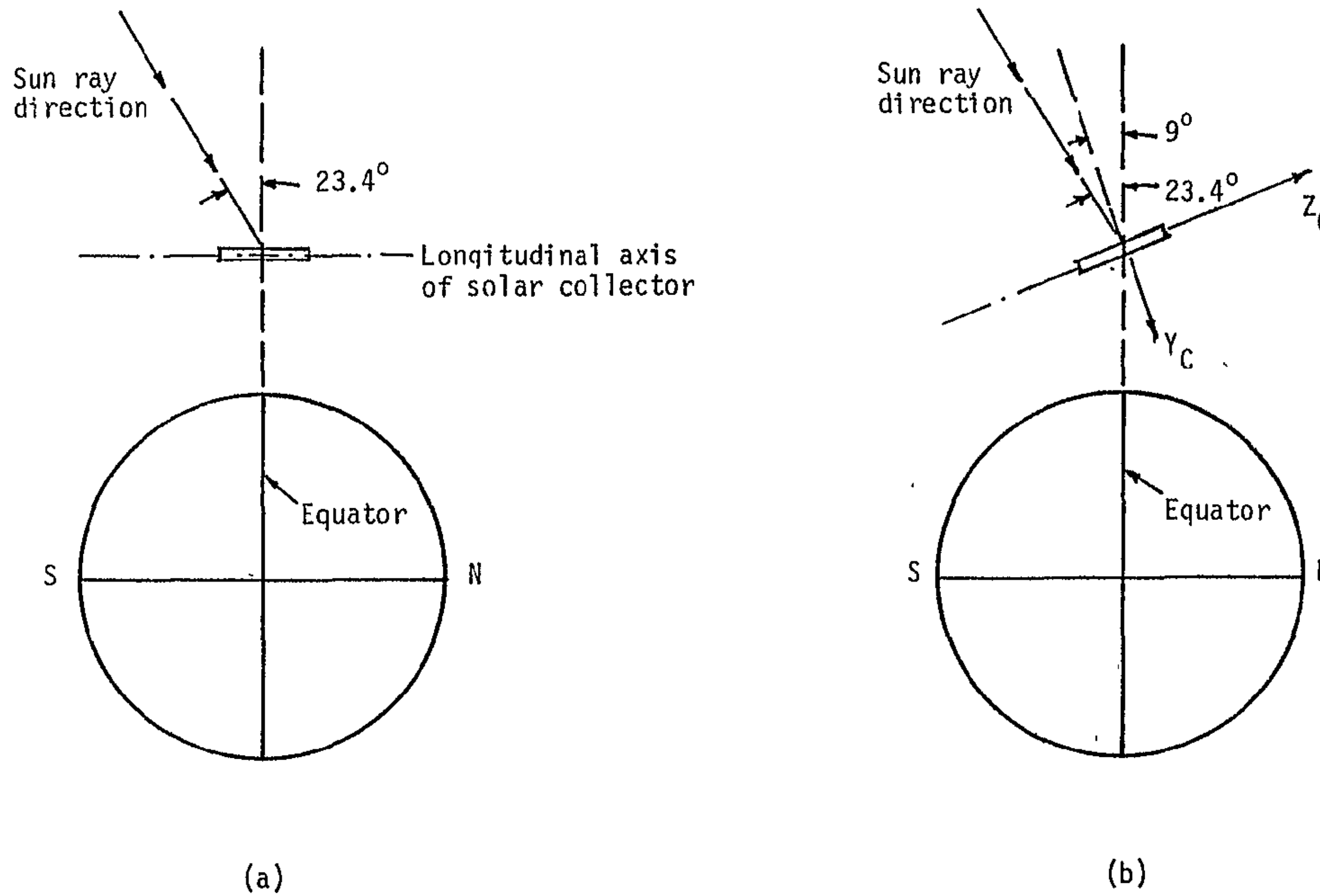

Figure 6.3-1. Solar collector attitude with satellite in geosynchronous orbit
(a) Zero gravity gradient torque attitude
(b) Nine-degree tilt attitude

isolated from the collector response even when bearings are frictionless.

7.0 COMMAND SIGNALS FOR ANTENNA CONTROL

7.1 Error Signals and Their Representation

In Section 5 the measured pointing error of the antenna was shown to be in the form of a pair of signals e_{ZA} and e_{XA}, representing tilt effects of the antenna disc about the Z_A and X_A axes, respectively. To correct this pointing error, command signals m_a and m_g are needed to turn the antenna and gimbal. Both m_a and m_g are to be generated from e_{ZA} and e_{XA}. Three approaches to the generation of command signals from sensed error signals will be proposed and discussed.

For the convenience of analysis, the antenna plane (Z_AX_A-plane) is adopted as an error plane, with Z_A and X_A axes representing errors e_{ZA} and e_{XA}, respectively. Therefore, corresponding to each antenna pointing error is a unique point on the antenna plane as shown in Fig. 7.1-1. If $\hat{u}$ is a unit vector along the center-to-center line between the antenna and rectenna as shown in Fig. 7.1-2, we can represent the pointing error geometrically as the projection of $\hat{u}$ on the antenna plane. Using this representation, the relationship between command signal and error signal can be obtained by successive uses of coordinate transformation.

Referring to Fig. 6.2-1, assume that when the antenna pointing error is zero, the antenna shaft angle and gimbal shaft angle are θ_{ao} and θ_{go}, respectively. With pointing errors, the respective angles are

$$\theta_{a1} = \theta_{ao} + \Delta\theta_a \qquad (7.1\text{-}1)$$

$$\theta_{g1} = \theta_{go} + \Delta\theta_g \qquad (7.1\text{-}2)$$

where $\Delta\theta_a$ and $\Delta\theta_g$ are angular perturbations which should be nulled for errorless pointing. The desired command signals are therefore,

$$m_a = -\Delta\theta_a \qquad (7.1\text{-}3)$$

$$m_g = -\Delta\theta_g \qquad (7.1\text{-}4)$$

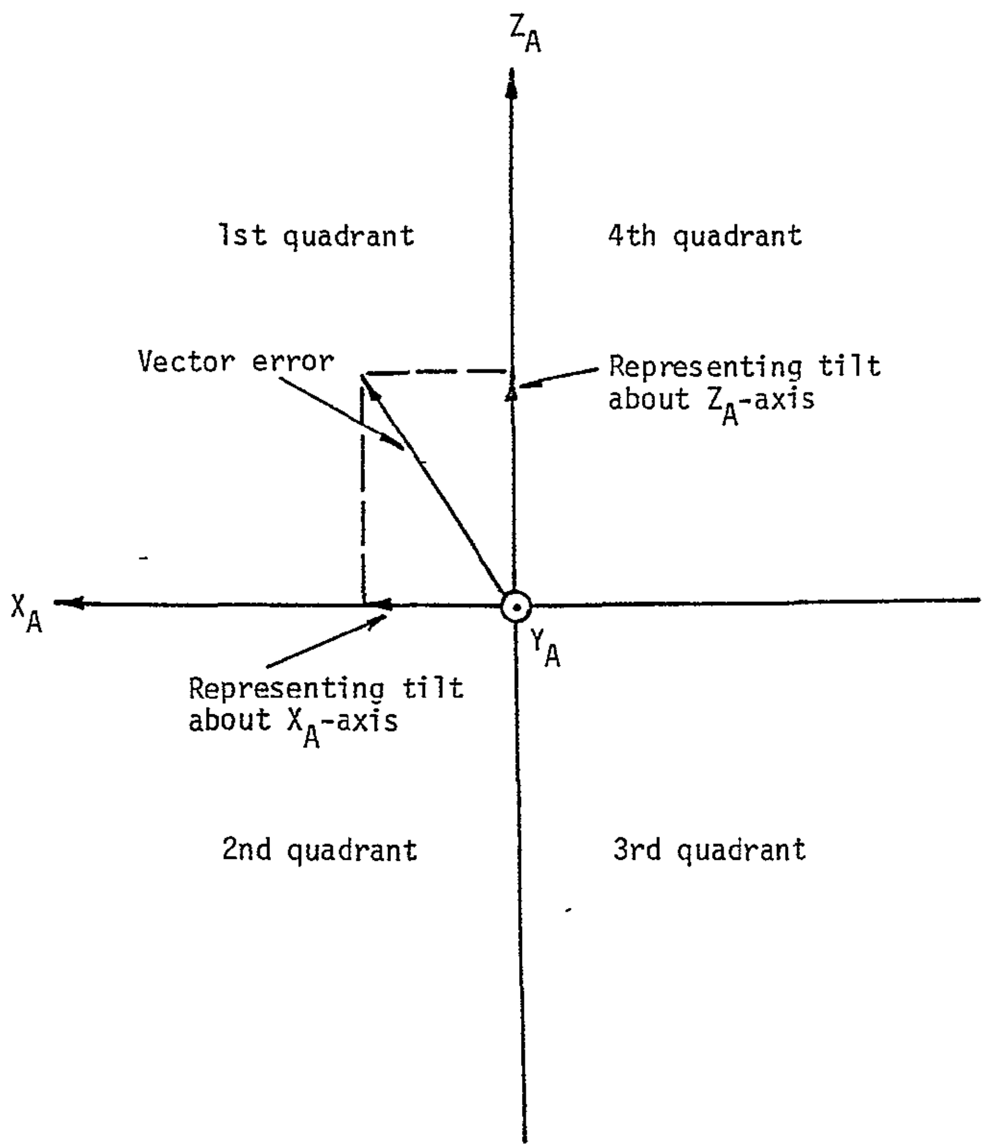

Figure 7.1-1. Antenna plane as error plane

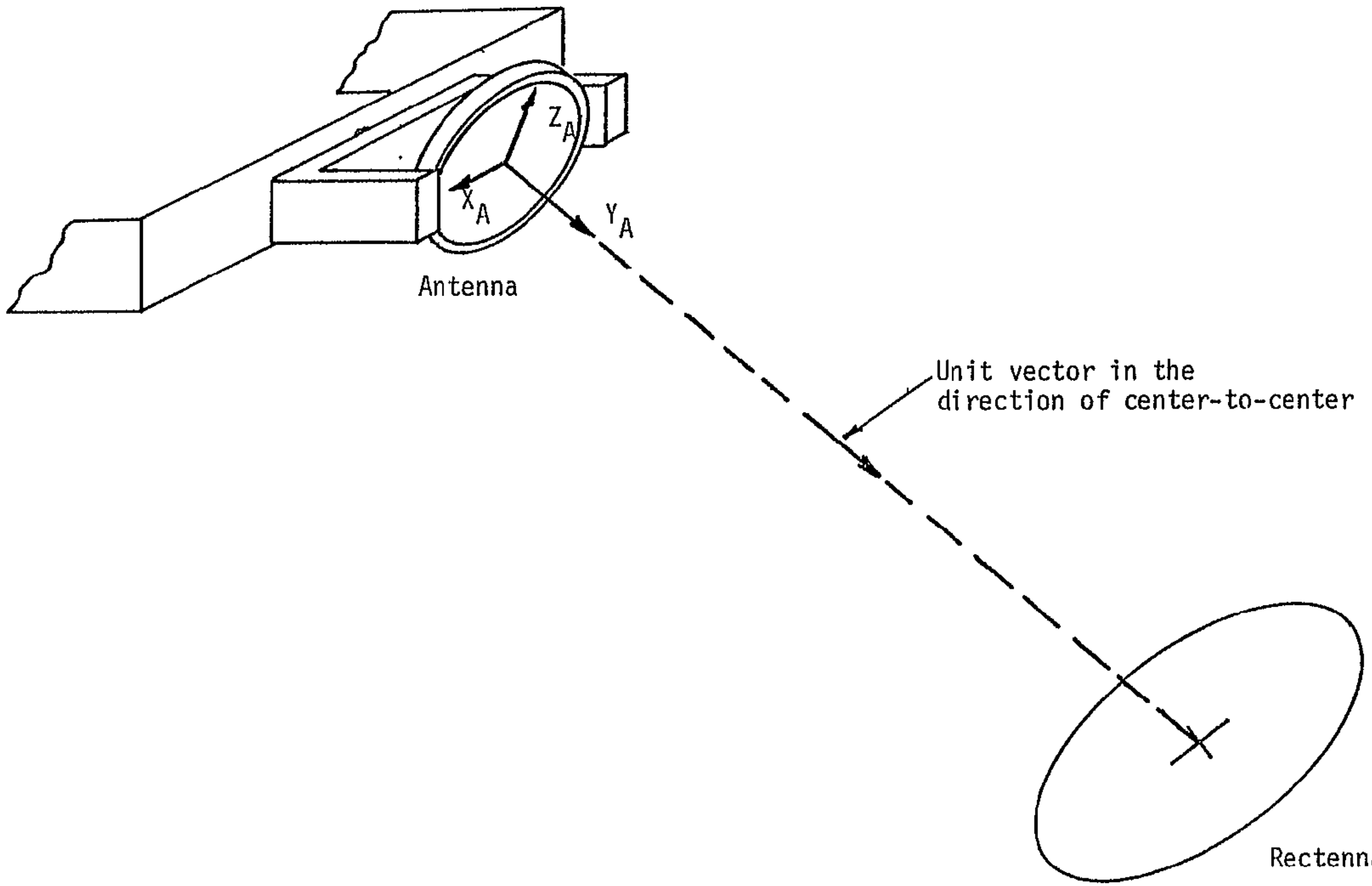

Figure 7.1-2. Projection representation of pointing error

7.2 Command Signals by On-line Analytic Solution

When the antenna has a pointing error, the projection of $\hat{u}$, the center-to-center unit vector between antenna and rectenna, on the antenna plane is non-zero. We are interested in determining the functional relationship between the projection and a given set of $\Delta\theta_a$ and $\Delta\theta_g$.

The unit vector $\hat{u}$ expressed in perfectly aligned antenna coordinate frame is

$$\hat{u}_{Ao} = \begin{bmatrix} 0 \\ 1 \\ 0 \end{bmatrix}. \tag{7.2-1}$$

Rotating the antenna about its shaft from θ_{ao} to $\theta_{a1} = \theta_{ao} + \Delta\theta_a$, the $\hat{u}$ expressed in the antenna frame becomes

$$\hat{u}_{A1} = T_1 \; \hat{u}_{Ao} , \tag{7.2-2}$$

where

$$T_1 = \begin{bmatrix} 1 & 0 & 0 \\ 0 & \cos\Delta\theta_a & \sin\Delta\theta_a \\ 0 & -\sin\Delta\theta_a & \cos\Delta\theta_a \end{bmatrix}. \tag{7.2-3}$$

The $\hat{u}$ vector expressed in the gimbal coordinate frame is

$$\hat{u}_{g1} = T_2 \; \hat{u}_{a1} \tag{7.2-4}$$

where

$$T_2 = \begin{bmatrix} 1 & 0 & 0 \\ 0 & \cos\theta_{a1} & -\sin\theta_{a1} \\ 0 & \sin\theta_{a1} & \cos\theta_{a1} \end{bmatrix}. \tag{7.2-5}$$

Rotating the gimbal about its shaft from θ_{go} to $\theta_{g1} = \theta_{go} + \Delta\theta_g$, the $\hat{u}$ expressed in gimbal frame becomes

$$\hat{u}_{g2} = T_3 \; \hat{u}_{g1} \tag{7.2-6}$$

where

$$T_3 = \begin{bmatrix} \cos\Delta\theta_g & \sin\Delta\theta_g & 0 \\ -\sin\Delta\theta_g & \cos\Delta\theta_g & 0 \\ 0 & 0 & 1 \end{bmatrix}. \tag{7.2-7}$$

Now the antenna and gimbal have been rotated about their respective axes by $\Delta\theta_a$

and $\Delta\theta_g$. The projection of unit vector $\hat{u}$ on the antenna plane is

$$\hat{u}_{a2} = T_2^t \ \hat{u}_{g2} = T_2^t \ T_3 \ T_2 \ T_1 \ \hat{u}_{ao} \tag{7.2-8}$$

If the three components of $\hat{u}_{A2}$ are p_{XA}, p_{YA} and p_{ZA}, the projections of $\hat{u}$ on three coordinates of the antenna frame are

$$p_{XA} = \sin\Delta\theta_g \cos\theta_{a1} \cos\Delta\theta_a + \sin\Delta\theta_g \sin\theta_{a1} \sin\Delta\theta_a \tag{7.2-9}$$

$$\begin{aligned} p_{YA} = {} & \cos\Delta\theta_g \cos\Delta\theta_a \cos^2\theta_{a1} + \sin^2\theta_{a1} \cos\Delta\theta_a \\ & + \cos\Delta\theta_g \cos\theta_{a1} \sin\theta_{a1} \sin\Delta\theta_a - \sin\theta_{a1} \cos\theta_{a1} \sin\Delta\theta_a \end{aligned} \tag{7.2-10}$$

$$\begin{aligned} p_{ZA} = {} & -\cos\Delta\theta_g \sin\theta_{a1} \cos\theta_{a1} \cos\Delta\theta_a + \cos\theta_{a1} \sin\theta_{a1} \cos\Delta\theta_a \\ & + \cos\Delta\theta_g \sin^2\theta_{a1} \sin\Delta\theta_a - \cos^2\theta_{a1} \sin\Delta\theta_a . \end{aligned} \tag{7.2-11}$$

Projections p_{XA} and p_{ZA} are directly proportional to the error signals e_{XA} and e_{ZA}, that is,

$$p_{XA} = k \ e_{ZA} \tag{7.2-12}$$

and

$$p_{ZA} = k \ e_{XA} \tag{7.2-13}$$

They are also related to antenna tilt angles $\Delta\theta_{XA}$ and $\Delta\theta_{ZA}$ by

$$p_{XA} = \sin \Delta\theta_{ZA} \tag{7.2-14}$$

and

$$p_{ZA} = -\sin \Delta\theta_{XA} \tag{7.2-15}$$

for small $\Delta\theta_{ZA}$ and $\Delta\theta_{XA}$. Therefore,

$$k \ e_{XA} = \sin \Delta\theta_{ZA} \tag{7.2-16}$$

$$k \ e_{ZA} = \sin \Delta\theta_{ZA} \tag{7.2-17}$$

For large tilt angles, vector representation is not valid. Eq. (7.2-10) will not be used since p_{YA} is not related to the measured pointing error. Equating (7.2-14) to (7.2-9) and (7.2-15) to (7.2-11) and simplifying gives the results

$$\sin\Delta\theta_{ZA} = \sin\Delta\theta_g \cos\theta_{ao} \tag{7.2-18}$$

and

$$\sin\Delta\theta_{XA} = \sin\Delta\theta_a(\sin^2\theta_{ao} + \cos\Delta\theta_g \cos^2\theta_{ao})$$

$$- \cos\Delta\theta_a(1 - \cos\Delta\theta_g) \cos\theta_{ao} \sin\theta_{ao}. \qquad (7.2\text{-}19)$$

To get command signals, $\Delta\theta_a$ and $\Delta\theta_g$ need to be obtained from tilt angles $\Delta\theta_{XA}$ and $\Delta\theta_{ZA}$ by solving (7.2-18) and (7.2-19). These two equations are nonlinear; therefore, the solution set is not unique, which is indeed true physically.

If the pointing error is sufficiently small so that the small angle approximations

$$\cos\Delta\theta \simeq 1 \text{ and } \sin\Delta\theta \simeq \Delta\theta \qquad (7.2\text{-}20)$$

are valid for $\Delta\theta_a$, $\Delta\theta_g$, $\Delta\theta_{ZA}$ and $\Delta\theta_{XA}$, then equations (7.2-18) and (7.2-19) reduce to

$$\Delta\theta_{ZA} = \Delta\theta_g \cos\theta_{ao} \qquad (7.2\text{-}21)$$

$$\Delta\theta_{XA} = \Delta\theta_a. \qquad (7.2\text{-}22)$$

Using the small angle approximation version of Equations (7.2-16) and (7.2-17) in (7.1-3) and (7.1-4), command signals are related to measured errors by

$$m_g = - \Delta\theta_g = - \frac{k}{\cos\theta_{ao}} e_{ZA} \qquad (7.2\text{-}23)$$

and

$$m_a = - \Delta\theta_a = - k\, e_{XA}. \qquad (7.2\text{-}24)$$

Notice that for situations where small angle approximations are valid the solution for command signals is unique.

7.3 Command Signal by Null-Seeking

For large pointing error the analytic means for command signals requires the solution of the nonlinear equations (7.2-18) and (7.2-19), which is not a simple task. Under this condition a null-seeking approach may be more practical.

When the unit vector $\hat{u}$ is not aligned with Y_A-axis of the antenna coordinate frame its projection on the antenna plane will be in one of the four quadiants formed by Z_A and X_A axes as shown in Fig. 7.3-1(a). Carefully studying Fig. 6.1-1, we find that the projection of $\hat{u}$ on antenna can be nulled by a sequential rotation of gimbal and antenna as follows:

(1) Rotate the gimbal about Z_G axis until the projection lines up with Z_A axis on the antenna plane.

(2) Rotate the antenna about X_A axis until the projection is zero.

The directions of rotation are determined according to the logic table shown in Fig. 7.3-1(b). The amount of rotations for gimbal and antenna depends on the initial position of the projection on the antenna plane in the following way.

- The closer the projection is to the X_A axis the more the gimbal rotation is needed
- The longer the projection vector is the more the antenna rotation is needed

This sequential null-seeking scheme is applicable to all pointing errors, large and small. It does not require computation for a solution of nonlinear equations. The scheme is suitable for compensating pointing-error-caused system anomalies and outside disturbances which vary slowly.

For small pointing errors, the effects of gimbal and antenna rotations are not coupled. The control sequences for $\Delta\theta_g$ and $\Delta\theta_a$ can be performed simultaneously and proportionally to the components of projection on Z_A and X_A axes.

7.4 Command Signals by Table-Lookup

Both of the above two approaches act slowly for large pointing errors - the analytic solution approach is slow because of the computation needed, while the null-seeking approach is slow because of its sequential nature.

Command signals can also be obtained by a table-lookup scheme. In this scheme, sets of command signals corresponding to their respective pointing errors are

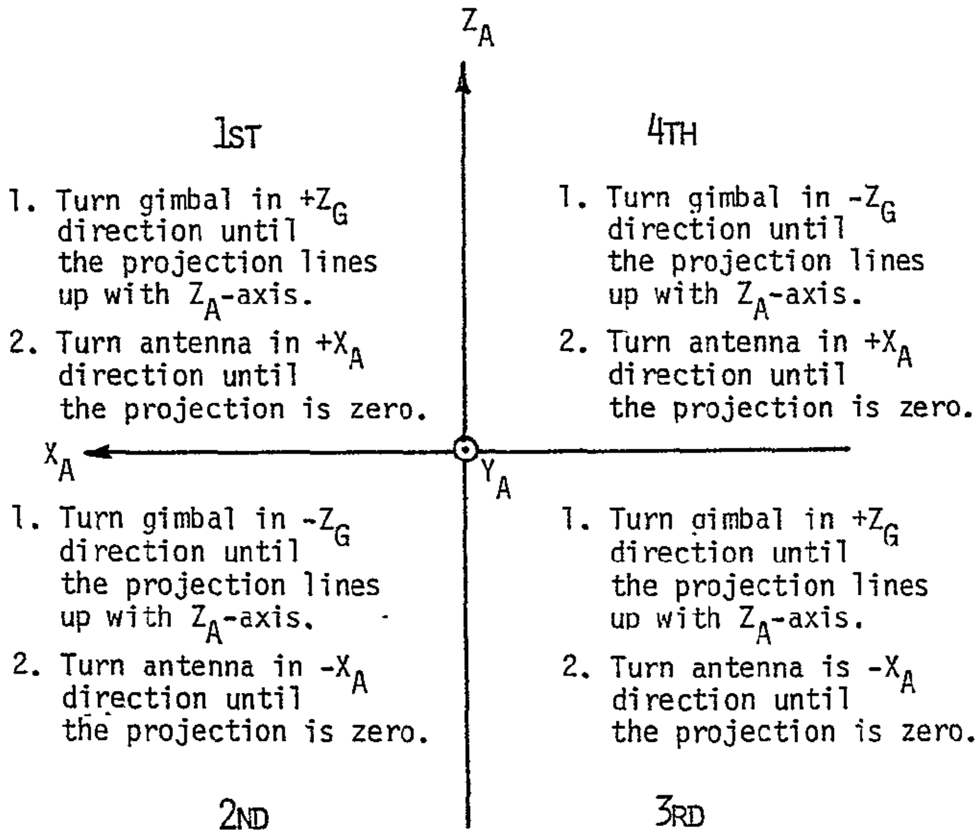

(a)

Quadrant where the projection is	1st	2nd	3rd	4th
Direction of gimbal rotation about Z_G-axis	+	-	+	-
Direction of antenna rotation about X_A-axis	+	-	-	+

(b)

Figure 7.3-1. Null-seeking command signal generation
(a) Four quadrants of antenna plane
(b) Command signal decision logic

precomputed and stored in the computer memory. If the size of table is not large, this is a fast method to generate command signals. The size of the table depends on the required resolution.

8.0 POINTING CONTROL SYSTEM

8.1 Flexible Body Nature of Solar Collector

As mentioned before, the activities of station-keeping and attitude control contribute to disturbing perturbations for antenna pointing control. Furthermore the action-and-reaction effect due to torquing complicates the pointing control especially when the flexible body modes of the solar collector and antenna disc can easily be excited. An analysis of pointing control dynamics requires knowledge of the flexible models concerned. Modeling the flexible body characteristics for solar collector and antenna is beyond the scope of present study. However, we need some kind of model for our pointing control system analysis. This section gives a crude development of torsion dynamics for the solar collector. We shall begin with a distributed parameter analysis and then approximate it by a lumped parameter model for future convenience. The bending dynamics of the collector, which is important, will not be discussed.

Let us approximate the solar collector by a uniform rectangular slab. Referring to Fig. 8.1-1 the following quantities are defined.

M —— density

E —— modulus of elasticty in shear

$A(Z)$ —— cross-section area

$J(Z)$ —— moment of inertia of area $A(Z)$ about Z axis

$I(Z)$ —— moment of inertia

Θ —— torsion angle

$\omega = \frac{\partial \Theta}{\partial t}$ —— torsion rate

T —— Torque

To begin, we shall assume zero damping. From a strength of material formula,

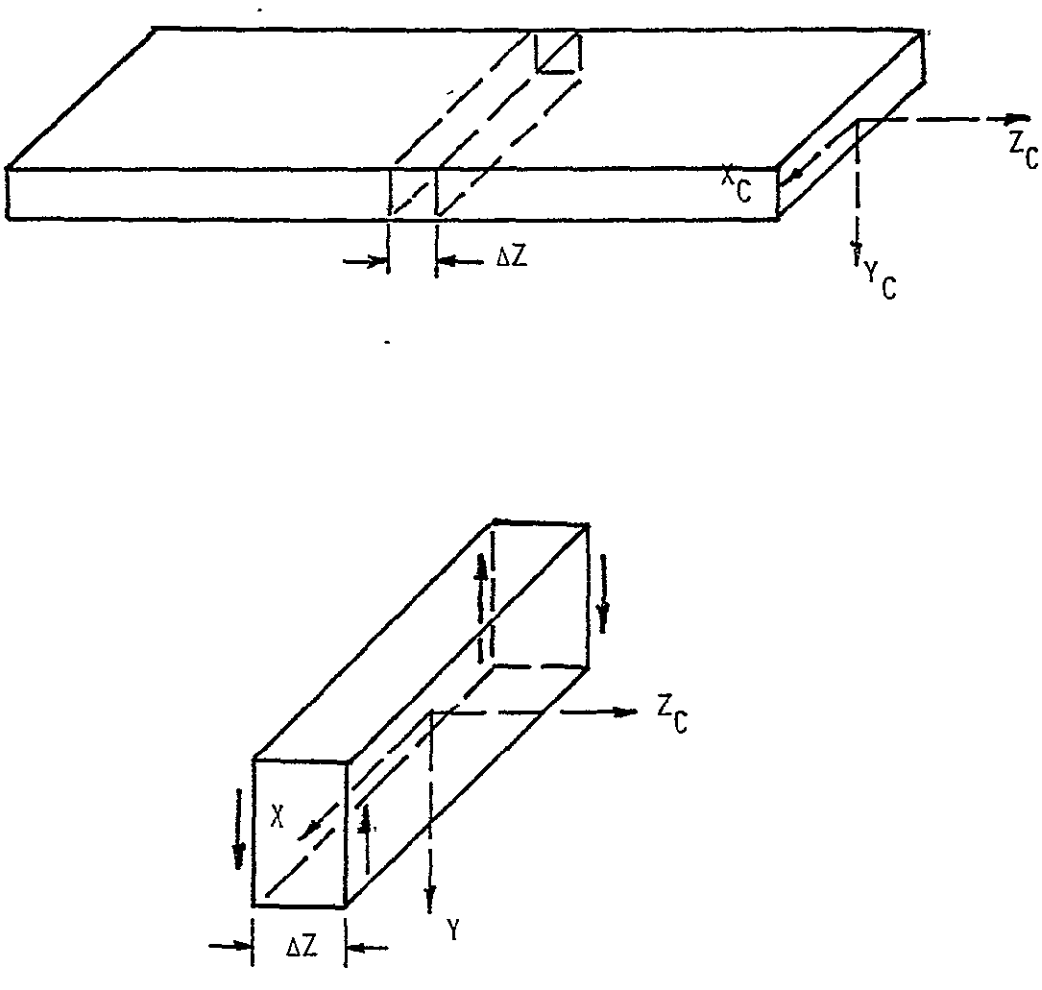

Figure 8.1-1. Torsion in solar collector

$$\Delta\Theta = \frac{T}{EJ}\ \Delta Z. \tag{8.1-1}$$

In the limit,

$$\frac{T}{EJ} = \frac{\partial\theta}{\partial Z} \ . \tag{8.1-2}$$

Taking the partial derivative with respect to time t,

$$\frac{1}{EJ}\frac{\partial T}{\partial t} = \frac{\partial\omega}{\partial Z} \ . \tag{8.1-3}$$

For a section of slab, ΔZ long; the Newton's second law of motion gives

$$\Delta I\ \frac{\partial\omega}{\partial t} = \Delta T. \tag{8.1-4}$$

but

$$\Delta I = mJ\Delta Z. \tag{8.1-5}$$

Hence

$$mJ\ \frac{\partial\omega}{\partial t} = \frac{\partial T}{\partial Z} \tag{8.1-6}$$

Equations (8.1-3) and (8.1-4) are two first order partial differential equations representing the torsion dynamics of the slab. By eliminating the torque T from these two equation, we obtain a second order partial differential equation for torsion rate:

$$\frac{\partial^2\omega}{\partial t^2} = \frac{E}{m}\ \frac{\partial^2\omega}{\partial Z^2} \ . \tag{8.1-7}$$

An equivalent equation for (8.1-7) is

$$\frac{\partial^2\Theta}{\partial t^2} = \frac{E}{M}\frac{\partial^2\Theta}{\partial Z^2} \quad . \tag{8.1-8}$$

With the inclusion of damping effects, (8.1-3) and (8.1-6) become

$$\frac{\partial\omega}{\partial Z} = \frac{1}{EJ}\ \frac{\partial T}{\partial t} + gT \tag{8.1-9}$$

$$\frac{\partial T}{\partial Z} = MJ\ \frac{\partial\omega}{\partial t} + f\omega \ . \tag{8.1-10}$$

where g and f are damping coefficients.

The solution of partial differential equations representing a distributed parameter system is, in general in the form of an infinite series which is not convenient for the study of pointing control.

To simplify the mathematics, let us use a lumped-parameter approximation for the distributed-parameter model, as shown in Fig. 8.1-2(a), which consists of two masses and one spring. An electric analogous network can be drawn for this system as shown in Fig. 8.1-2(b). The network equations, in Laplace transform, are

$$\left.\begin{aligned} T &= \Omega_1\ (sI_1 + \frac{E}{s}) - \Omega_2\ (\frac{E}{s}) \\ &\text{and} \\ 0 &= -\ \Omega_1\ (\frac{E}{s}) + \Omega_2\ (sI_1 + \frac{E}{s}) \end{aligned}\right\} \tag{8.1-11}$$

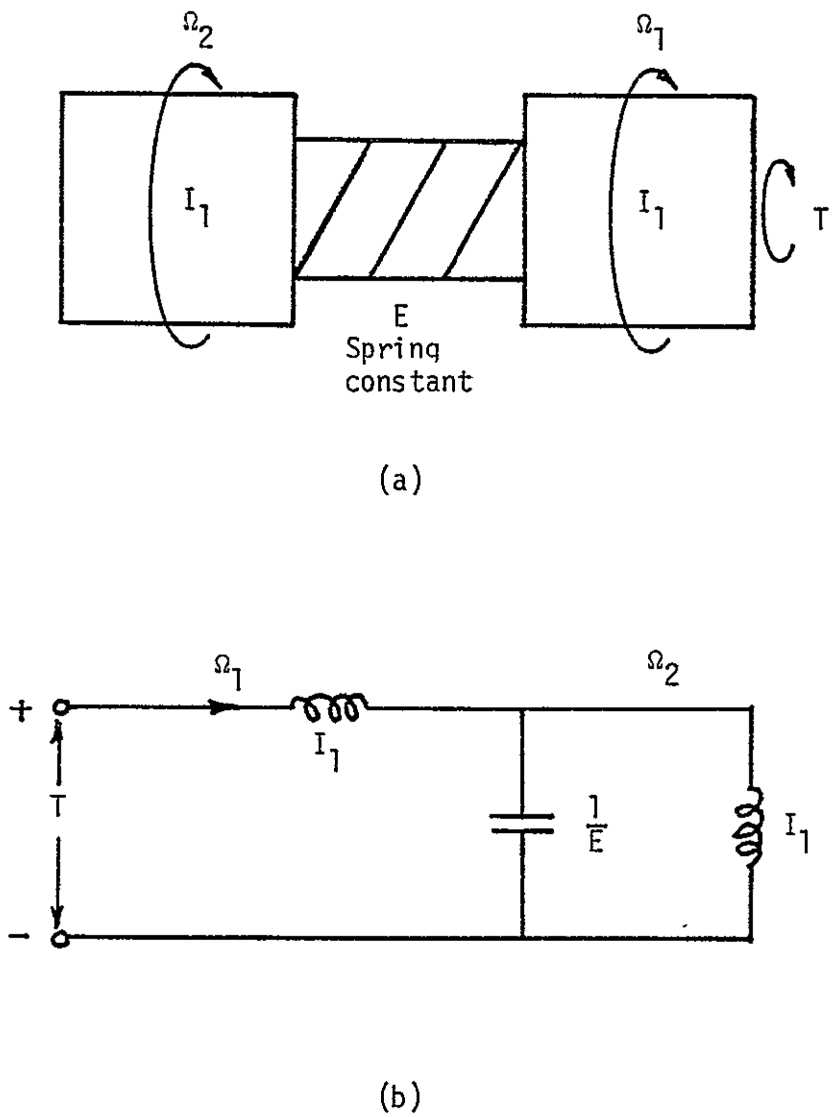

Figure 8.1-2. Lumped-parameter model

with a characteristic equation

$$\Delta = (sI + \frac{E}{s})^2 - (\frac{E}{s})^2 = s^2I^2 + 2\ EI \tag{8.1-12}$$

The response of angular rate at driving end in response to torque T(s) is

$$\Omega_1(s) = \frac{sI_1 + \frac{E}{s}}{s^2I_1^2 + 2\ EI_1}\ T(s) \tag{8.1-13}$$

The mechanical impedance of this mechanical network having a torque input at one end is

$$Z_e(s) = \frac{\Omega_1(s)}{T(s)} = \frac{sI_1 + \frac{E}{s}}{s^2{I_1}^2 + 2\ EI_1} \tag{8.1-14}$$

showing a pair of imaginary poles

$$s = \pm\ j\ \frac{E}{I} \tag{8.1-15}$$

If damping exists in the torsion model it can also be included in the analogous electric network. The effect is to shift the pair of imaginary pole into the left-half s-plane.

8.2 Torquer Characteristics

We shall now consider using d-c motor types of torquers for antenna pointing control. The torquer characteristic, namely, the torque versus speed relationship, affects the dynamics of pointing control. Three representative torquer characteristics are shown in Fig. 8.2-1. In general, the torquer characteristic is nonlinear as shown in Fig. 8.2-1(a). The

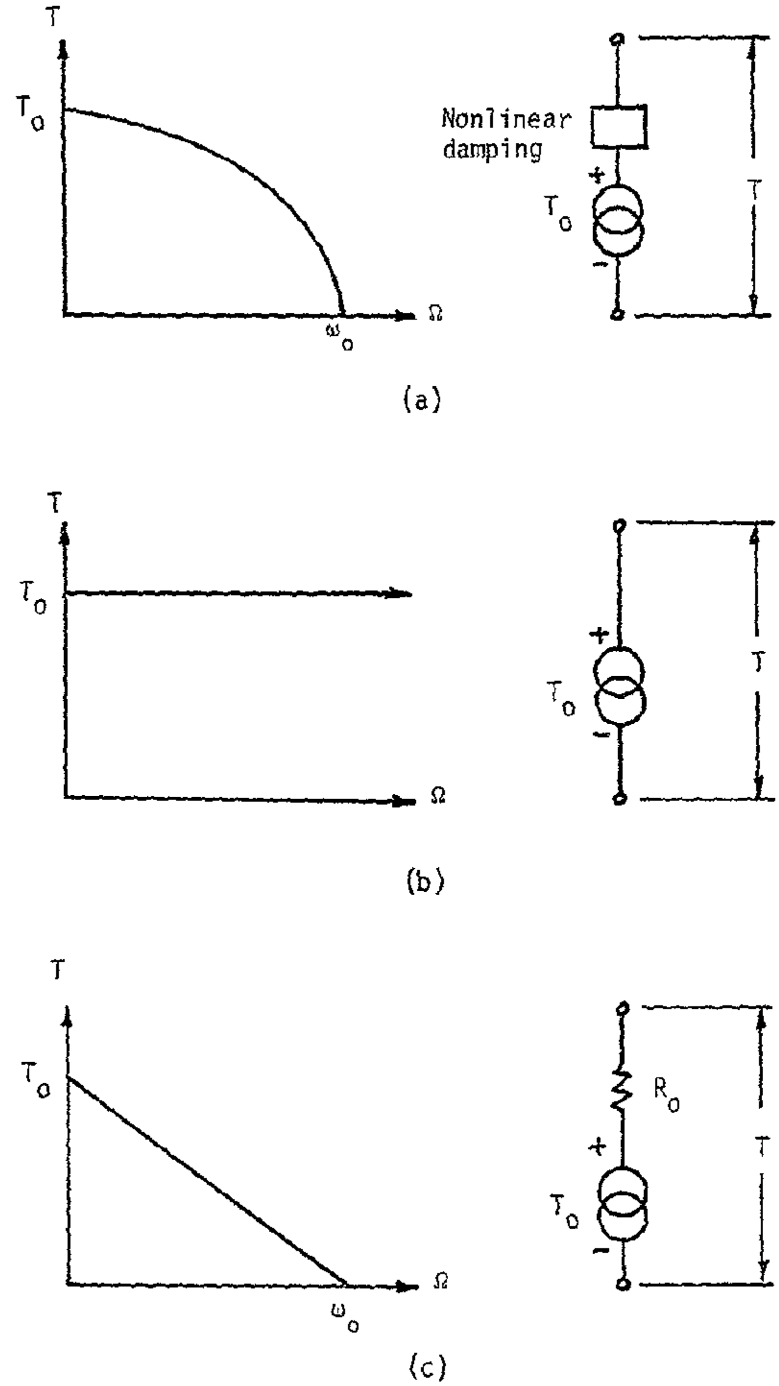

Figure 8.2-1. Torquer characteristics

form of nonlinearity depends on the field excitation arrangement, core material, structural configuration of field, armature, and air gap. An equivalent network for such a characteristic is a constant torque source T_0 in series with a nonlinear damping element. By appropriate use of both shunt and series excitations it is possible to approximate an ideal torquer characteristic which, for constant armature voltage, has a constant torque at all speed as shown in Fig. 8.2-1(b). The use of an ideal torquer decuples the dynamics of the antenna from that of the solar collector, which simplifies the pointing control problem. The equivalent network of an ideal torquer is simply a Torque source T_0. There are, however, practical considerations involved in adopting an ideal Torquer, such as the complexity of the d-c motor, energy consumption, and cost.

The most often used d-c motors have linear torque characteristics as shown in Fig. 8.2-1(c). The associated equivalent network is a torque source T_0 in series with a damping $R_0 = \frac{T_0}{\omega_0}$, where T_0 is the motor output torque at zero speed and ω_0 the speed of the motor at zero output torque. Physically this type of d-c motor is shunt excited and armature voltage controlled. For a constant armature voltage V, the torque-speed relationship is given by

$$T(t) = \frac{K_t}{R_a} V - \frac{K_t K_e}{R_a} \omega(t), \tag{8.2-1}$$

where K_t is motor torque constant, K_e is motor back-emf constant, and R_a is motor armature resistance. Matching Eq. (8.2-1) to Fig 8.2-1(c) gives

$$T_0 = \frac{K_t V}{R_a} \quad , \tag{8.2-2}$$

$$\omega_0 = \frac{V}{K_e} \quad , \tag{8.2-3}$$

and

$$R_0 = \frac{K_t K_e}{R_a} \quad . \tag{8.2-4}$$

8.3 One-Dimensional Plant Dynamics

We shall now restrict our discussion to a one-dimensional antenna pointing control, namely, the control of rotation about the Z_G-axis. The purpose is to gain insights about the point control dynamics. We assume a symmetric structure for the antenna and ignore all its flexible body and damping effects.

The one-dimensional pointing control structure is shown in Fig. 8.3-1. Notice that the motor speed ω is the relative speed of its armature side with respect to its field side. Since one side is fixed to the collector and the other side to the antenna, the motor speed is related to the collector speed ω_c and antenna speed ω_a by

$$\omega = \omega_a - \omega_c \quad . \tag{8.3-1}$$

Analogous electric networks for the system are given in Fig. 8.3-2. The effect of the antenna's moment of inertia I_a is represented by a mechanical impedance

$$Z_a = sI_a \quad . \tag{8.3-2}$$

Mechanical impedance for the collector has been obtained as

$$Z_c = \frac{sI_1 + \frac{E}{s}}{s^2 I_1^{\,2} + s\,EI_1} \quad . \tag{8.3-3}$$

With the torquer characteristics given by Eq. (8.2-1) we are ready for formulating the system equations.

The torquer input is voltage V and its output is torque T or speed ω.

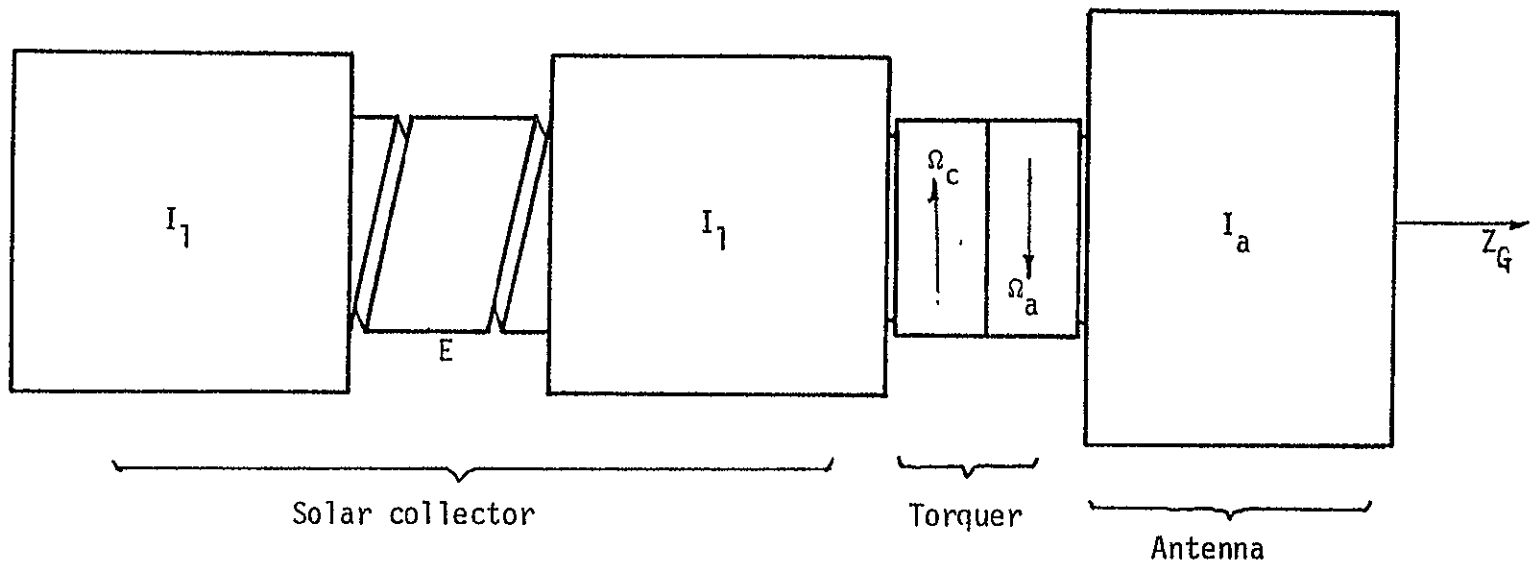

Figure 8.3-1. One dimensional plant

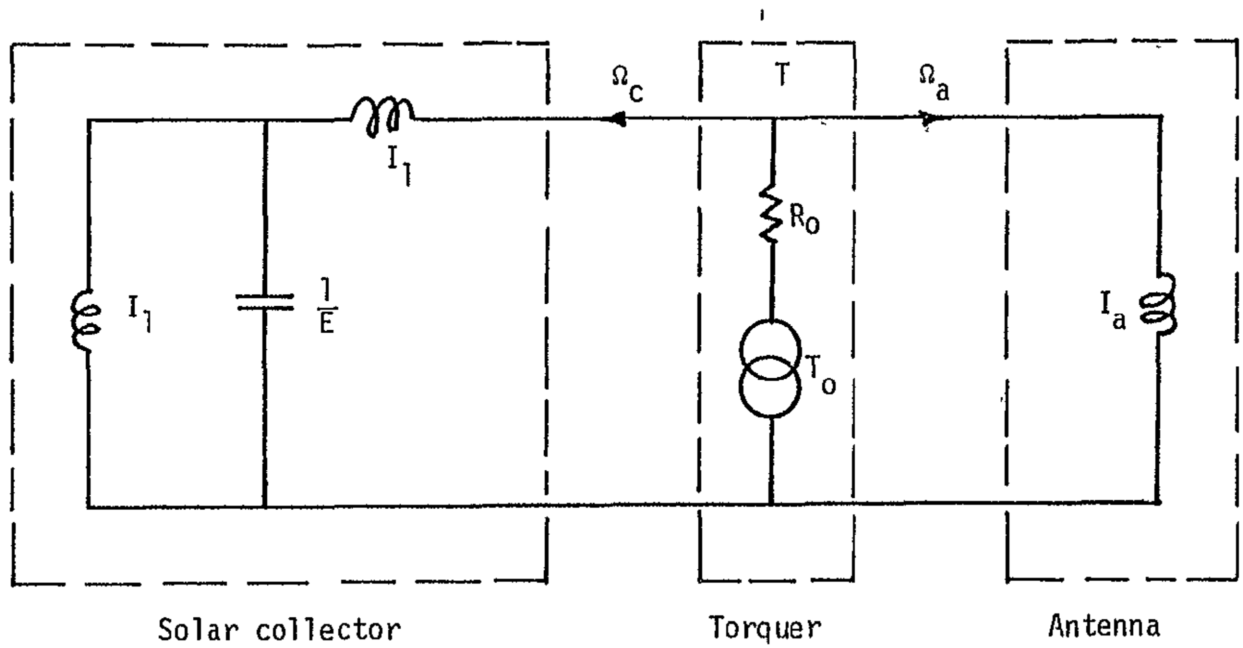

Figure 8.3-2. Equivalent circuit for the one dimensional plant

Substituting Eq. (8.3-1) into (8.2-1) gives

$$T(s) = \frac{K_t}{R_a} V(s) - \frac{K_t K_e}{R_a} [\Omega_a(s) - \Omega_c(s)]. \tag{8.3-4}$$

Notice that Ω_a and Ω_c are physically in opposite directions as shown in Fig. 8.3-1. Therefore

$$T(s) = \Omega_a(s) Z_a (s) \quad , \tag{8.3-5}$$

$$T(s) = - \Omega_c(s) Z_c(s) \quad , \tag{8.3-6}$$

and

$$\Omega_c(s) = - \frac{Z_a(s)}{Z_c(s)} \Omega_a(s) . \tag{8.3-7}$$

Substituting Eq. (8.3-5) into the left-hand side of (8.3-4) and Eq. (8.3-7) into the right-hand side and rearranging terms, we get

$$\frac{\Omega_a(s)}{V(s)} = \frac{\frac{1}{K_e}}{1 + \frac{Z_a(s)}{Z_c(s)} + \frac{Z_a(S)}{R_o}} \tag{8.3-8}$$

$$\frac{\theta_g(s)}{V(s)} = \frac{\frac{1}{K_e}}{s\left[1 + \frac{Z_a(s)}{Z_c(s)} + \frac{Z_a(s)}{R_o}\right]} \tag{8.3-9}$$

Eq. (8.3-8) is the transfer function from the torquer control voltage to the antenna's turning rate about Z_G-axis. Loading effects due to both the antenna and solar collector are included in this transfer function.

By using $Z_a(s)$ and $Z_c(s)$, as given by Equations (8.3-2) and (8.3-3), in (8.3-8) we obtain the transfer function in terms of system parameters as follows:

$$\frac{\Omega_a(s)}{V(s)} = \frac{K\, R_o(s^2 + a_o)}{s^3 + R_o\, b_2\, s^2 + b_1\, s + R_o\, b_o} , \qquad (8.3\text{-}10)$$

where R_o is given in Eq. (8.2-4) and

$$\left.\begin{aligned} a_o &= \frac{2E}{I_1} , \\ b_o &= \frac{(2\, I_1 + I_a)E}{I_a I_1^2} , \\ b_1 &= \frac{2E}{I_1} , \\ b_2 &= \frac{I_1 + I_2}{I_a\, I_1} , \end{aligned}\right\} \qquad (8.3\text{-}11)$$

and

$$K = \frac{1}{K_e\, I_a} . \qquad (8.3\text{-}12)$$

Eq. (8.3-10) shows that the plant has a pair of imaginary zeros at

$$s = \pm\, j \sqrt{a_0}\ . \tag{8.3-13}$$

Poles of the plant are roots of

$$s^3 + R_o\, b_2\, s^2 + b_1\, s + R_o\, b_o = 0\ . \tag{8.3-14}$$

For $R_o = 0$, the roots are at

$$\left.\begin{aligned} &s = 0 \\ \text{and}\quad & \\ &s = \pm\, j \sqrt{b_1} = \pm\, j \sqrt{a_0} \end{aligned}\right\} \tag{8.3-15}$$

Poles and zeros at $\pm\, j \sqrt{a_0}$ cancel, leaving the plant as a pure integrator. For $R_o = \infty$, the plant reduces to a second order system with poles at

$$s = \pm\, j \sqrt{\frac{b_o}{b_2}} = \pm\, j\, \gamma \sqrt{a_o}\quad , \tag{8.3-16}$$

where

$$\gamma = \sqrt{\frac{I_1 + \frac{I_a}{2}}{I_1 + I_a}} < 1\quad . \tag{8.3-17}$$

For finite values of R_o, the plant has one real pole and a pair of complex conjugate poles, all on the left-half of the s-plane.

8.4 A Numerical Example

Consider the parameter values of antenna and solar collector as indicated in Fig. 8.4-1. For each one of the two collector blocks, the moment of inertia about the Z_G-axis is

$$I_1 = \frac{M(a^2 + b^2)}{12} = 17.33 \times 10^{12} \text{ kg-m}^2 \quad .$$

Let the modulus of elasticity for shear be

$$E = 8 \times 10^9 \text{ kg/m}^2 \quad .$$

The moment of inertia of the cross-section area is

$$J = \frac{1}{12} ab \, (a^2 + b^2) = 10.83 \times 10^{12} \text{ m}^4 \quad .$$

For a total torsion angle ϕ, from end to end of the collector, of 0.1 radian (5.73 degrees), the total torque from end to end is

$$T = \frac{\phi \times E \times J}{L} = 8.66 \times 10^{17} \text{ n-m} \quad .$$

Consider the antenna structure being a circular disc, then its moment of inertia about the diameter is

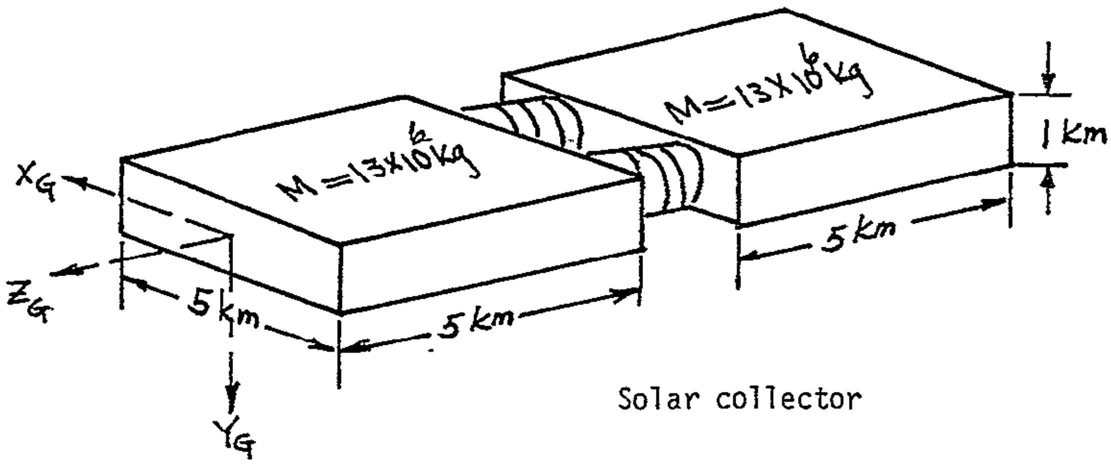

Solar collector

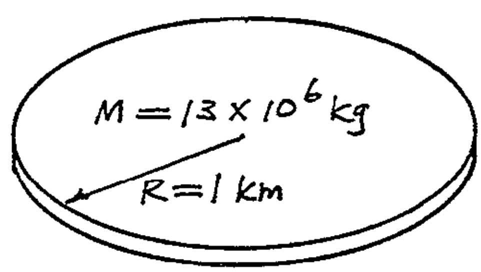

Antenna

Figure 8.4-1. Parameter values for the example

$$I_a = \frac{1}{4} MR^2 = 3.25 \times 10^{12} \text{ kg-m}^2$$

Using the above parameter values, equations (8-29) and (8-35) give

$$a_o = 9.23 \times 10^{-4} \quad ,$$

$$b_o = 3.10 \times 10^{-16} \quad ,$$

$$b_1 = 9.23 \times 10^{-4} \quad ,$$

$$b_2 = 3.66 \times 10^{-13} \quad ,$$

and

$$\gamma = 0.96.$$

The plant's zeros are at $s = \pm j\, 0.03$. Loci of its three poles as functions of torquer damping R_o are shown in Fig. 8.4-2. The existence of oscillatory low damping characteristics is evident. The proximity of complex poles to complex zeros implies low oscillation amplitude. Without further investigation, however, this should not be ignored in closed-loop system design because of the high precision requirement of the antenna pointing.

8.5 Pointing Control System Configuration

All the previous discussions are prerequisits to the development of a pointing control system for SPS. Fig. 8.5-1 depicts a configuration for

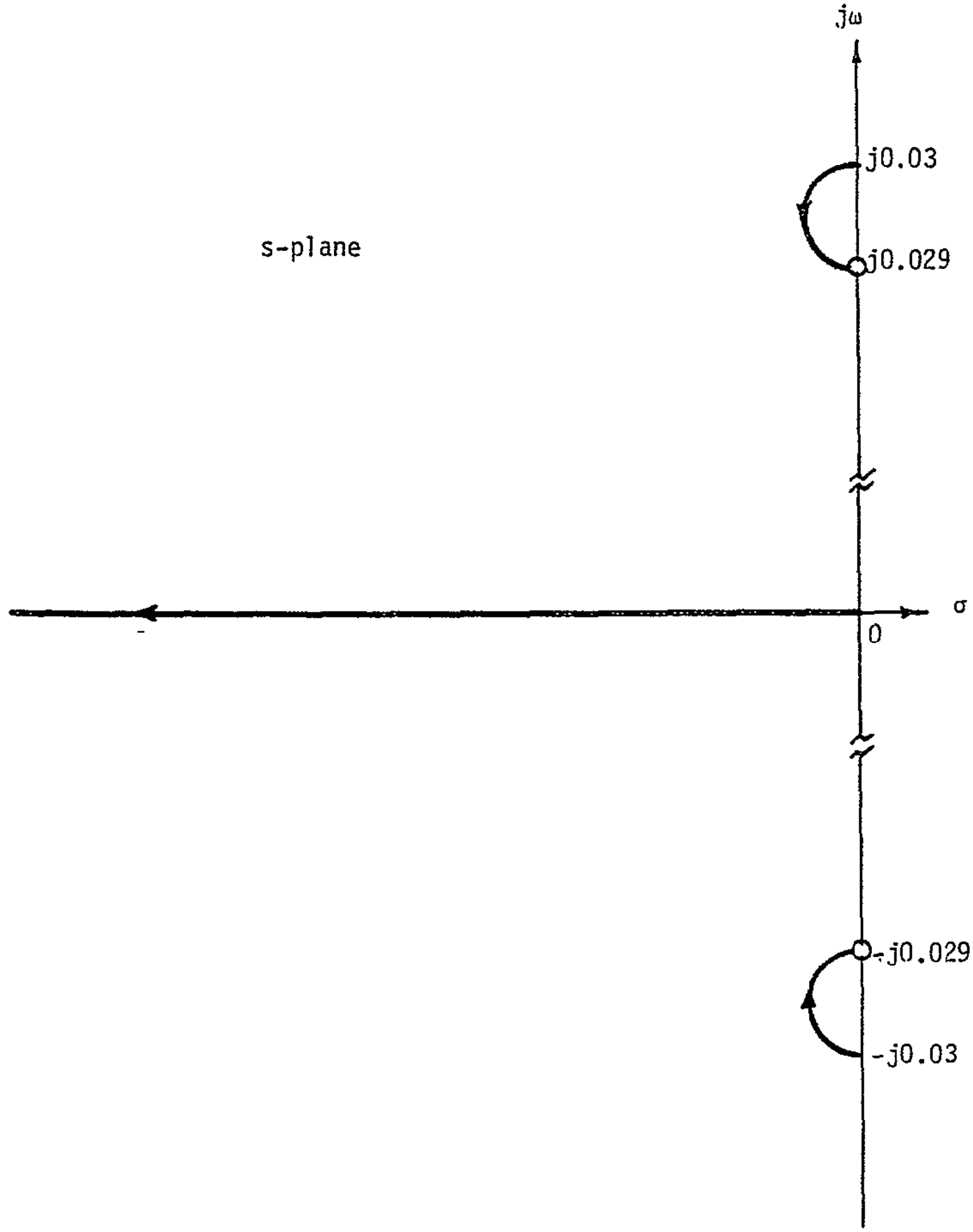

Figure 8.4-2. Root-loci of the plant for increasing R_0

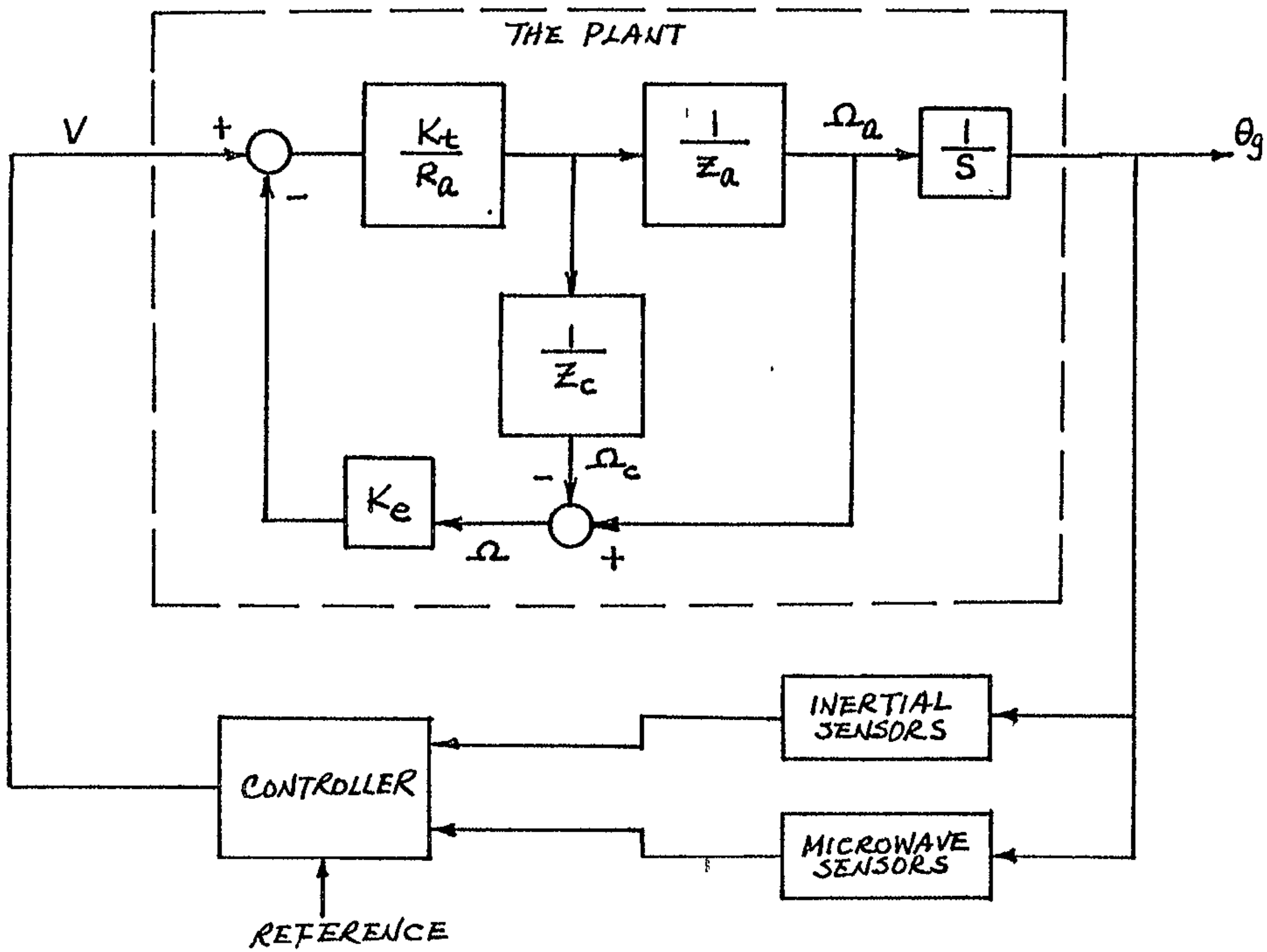

Figure 8.5-1. Pointing control system configuration

pointing control system. Notice that inertial sensors are included for antenna attitude measurement. They are needed to sense large attitude error which may be outside the range of microwave sensors.

9.0 CONCLUSIONS AND RECOMMENDATIONS

9.1 Conclusions

In the area of electronic pointing of the power beam it has been found that three basic components are required to implement the microwave retrodirective array (the PPG, RPD, and PCC components). One form of circuit was discussed to implement each component (Figures 3.1-1, 3.2-1, and 3.3-1). These circuits represent basic forms and a final realization of the system may be different for various practical reasons.

System electrical and mechanical errors that affect pointing error and power beam efficiency are outlined in Fig. 4.0-1. These power beam characteristics are primarily affected by errors generated at the subarray level. One of the most serious subarray mechanical errors is tilt. For one mode of vibration of the array face it is found that some subarrays undergo significant tilt (33.2% of the subarray beamwidth). Because of the complicated way in which tilt affects the power beam no detailed evaluation was made in this limited-scope study. However, it is felt that tilt due to vibration should mainly affect beam efficiency and sidelobes (not pointing accuracy).

Many other microwave-type errors were considered in the study. Most of these require a considerably greater level of detailed effort than available in this first-phase effort.

It was shown in section 5.0 that very little special hardware was required to implement the angle error sensors required by the gimbal servos. A simple error-sensing method was developed that required the hardware shown in Fig. 5.1-2 be available at each subarray.

The significant results in the investigation of mechanical pointing control are the following:

1. Three methods for the generation of command signals for torques, based on sensed error signals, are proposed. One can also use

a combination of these three methods for command signal generation.

2. A crude analysis of the effect of flexible body characteristics of the solar collector on the overall SPS plant characteristics for pointing control.
3. A control system configuration for pointing control is given in the form of a block diagram.

9.2 Recommendations

The following list constitutes the principal areas that relate to electronic pointing control in SPS that should undergo more detailed study:

1. Many of the mechanical and electrical errors are difficult to analyze to determine their affect on accuracy and beam efficiency. It is suggested that a computer simulation could determine these effects. The simulation would not be an inexpensive tool since SPS is a complicated system. However, there may be no other way to evaluate some error sources short of actual construction.
2. A study should be made to determine a good architecture for signal distribution in SPS. This is especially applicable to the selection of the RPD component to minimize physical mass. It is also important in the PPG and PCC components to minimize signal interference due to leakages.
3. Analysis should be done on the architecture selected in part 2 to determine noise effects and to establish signal levels (signal-to-noise ratios) required in the system.
4. Additional evaluation of the suggested error sensing concept for gimbal servo control needs to be done to determine its sensitivity to errors in subarray phases and to see if some form of angle normalization is needed.

The following activities should be further pursued in regard to the development of a mechanical pointing control system for SPS:

1. Analysis of the torsion and bending characteristics of the solar collector.
2. Analysis of the wobbling characteristics of the antenna disc.
3. Analysis of the joint dynamics of the collector and antenna.
4. Analysis of the dynamic collector-antenna under closed-loop control. Investigate the condition of instability if any.
5. A more specific formulation of control parameters for required pointing control accuracy.
6. A study of the best control strategy or control law for a set of desired performance considerations.
7. Development of pointing control algorithm.
8. Pointing control system sensitivity analysis.
9. System simulation.